SELF-POWERED FIBER BRAGG GRATING SENSORS

by

Benjamin W. McMillen

B.S. Electrical Engineering, University of Pittsburgh 2003

Submitted to the Graduate Faculty of

The School of Engineering in partial fulfillment

of the requirements for the degree of

Master of Science in Electrical Engineering

University of Pittsburgh

2007

UNIVERSITY OF PITTSBURGH

SCHOOL OF ENGINEERING

This thesis was presented

by

Benmamin W. McMillen

It was defended on

July 18, 2007

and approved by

Dr. William Stanchina, Professor and Chairman, Department of Electrical and Computer Engineering

Dr. Joel Falk, Professor, Department of Electrical and Computer Engineering

Dr. Sung Kwon Cho, Assistant Professor, Department of Mechanical Engineering and Materials Science

Thesis Advisor: Dr. Kevin P. Chen, Paul E. Lego Assistant Professor, Department of Electrical and Computer Engineering

SELF-POWERED FIBER BRAGG GRATING SENSORS

Benjamin W. McMillen, M.S.

University of Pittsburgh, 2007

Fiber Bragg gratings (FBGs) are key components for optical sensing and communication. Traditionally, fiber grating sensors were purely passive, but recent developments have been made to allow active tuning of these sensors. These tuning methods, though effective, are often bulky, cumbersome, and expensive to package.

This thesis demonstrates an approach for tuning in-fiber Bragg grating sensors by optical energy carried by the same optical fiber. Optical energy carried by optical fiber was used to heat in-fiber Bragg gratings to alter grating response to surrounding media. This tuning technique requires no external actuation or expensive packaging. Through the use of a simple metallic film and the delivery of high power laser light to the grating, 'active' tuning is obtained.

Two applications are demonstrated where self-powered FBG technology is applied to a level sensor capable of measuring discrete liquid levels as well as a vacuum sensor, with sensitivity into the milli-torr range. These sensors are also a demonstration of the networkability of FBG sensor arrays, allowing for large multipoint sensor networks. In addition, both sensors have dual functionality, being capable of sensing local temperature in addition to vacuum and liquid levels. These sensors are comparable or better than most MEMS and fiber based technology.

Optical fiber in both these applications serves as a conduit for both signal-carrying light as well as power light, used to tune the gratings. This new self-powered FBG-based technology provides an innovative solution to fiber sensing, allowing design of versatile sensors without compromising their intrinsic benefits. Not only does the one-fiber solution provide lower design costs by utilizing a single feed through, but it also boasts simple packaging, long lifetime, reliable operation in harsh environments, and immunity to electromagnetic fields.

TABLE OF CONTENTS

LIST OF FIGURES

PREFACE

I would initially like to thank Dr. Kevin Chen, without the help of whom none of this would have been possible. I would also like to thank my parents for putting up with my ‘extended stay’ in college here at the University Of Pittsburgh. Thanks to Dr. Joel Falk, Dr. William Stanchina, and Dr. Sung Cho for agreeing to sit on my committee as well as Charles Jewart for his assistance in setting up and performing the various experiments outlined in this thesis.

1.0 INTRODUCTION

1.1 MOTIVATION

The discovery of fiber Bragg gratings (FBGs) in the late 1970s [1, 2] opened the floodgates for fiber communication networks and fiber based sensing. These simple devices were immediately recognized as key components in many applications as a result of their inherent advantages. Formed by an induced periodic index change in the core of an optical fiber, FBGs have seen use in dispersion compensation [3, 4], filtering [5-7], routing [8], and, most importantly, fiber sensing. In order to better understand the theory behind Bragg grating operation and fabrication, much research involving Bragg gratings and their applications has been undertaken.

When compared to traditional sensing techniques, many of the inherent advantages of an FBG based device immediately become apparent. Traditionally, sensing involves the use of a means of signal delivery to and from the sensing device, most often in the form of electrical cabling. This cabling, if not shielded, is susceptible to electromagnetic interference (EMI), which causes erroneous outputs on sensor readings. Though shielding may solve this problem, it adds weight and cost to a system. FBG-based devices, being purely optical, are immune to EMI and suffer no interference during operation. Because of their simplicity, fabrication of FBGs is a low-cost process. This simplicity not only contributes to lower cost and simpler packaging, but it also allows for a very long lifetime of the sensor. Since the makeup of an FBG-based device is silica, the sensor has the capability to operate in very harsh conditions for extended periods of time. Also, these devices may be tailored to have a varying range of sensitivity, making them ideal for nearly any sensing application or environment. Lastly, versatility is also a factor in making these devices highly appealing. Due to their small size and low insertion loss, FBG-based sensors placed in succession along the length of an optical fiber allow the creation of a multipoint sensing network. Sensors of varying types may be placed at strategic locations in the network, all requiring a single signal line.

One limiting factor in the use of fiber Bragg gratings in sensing is their total passivity. Bragg gratings are extremely sensitive to environmental factors such as temperature and strain, which make them ideal as sensors. These factors however, may have detrimental effects on the desired parameter being measured. For this reason, fiber sensors often include bulky electro-mechanical devices to compensate for undesired factors such as temperature drift, adjustment of sensitivity and set point [9]. The addition of tuning allows for an even greater realm of applications for fiber Bragg gratings and sensing techniques.

Though several tuning techniques have been presented [10-15], the common drawbacks of traditional sensing now become a factor in both cost and design. The proposed methods of tuning often require delicate packaging and the need for electrical signals and power to be carried to and from the Bragg grating sensor. These electrical signals provide control for mechanical actuators as well as provide power for resistive coatings, all of which are used as methods for tuning. In a sense, this is taking a step back. Now these sensors no longer have the inherent advantages that were viewed to be so appealing. The additional components added to the sensor not only drive up manufacturing cost, but also add bulk to the sensor making it unsuitable for large networks or tight locations. In addition, the delicate packaging and mechanical components spell disaster for longevity of the sensor, since the electrical components have a much shorter lifetime than that of silica fiber. Device application is now limited, since the sensors may not be able to function in harsh environments where high temperature changes or dynamic G forces are common. To make matters worse, the sensing system now must contend with EMI, which further limits the application of these sensors.

A solution to this problem has, however, been presented. Developed by Dr. Kevin P. Chen of the University of Pittsburgh, tunable gratings are now made possible, electrical cable free, through the use of in-fiber laser light [9]. In this tuning scheme, high power laser light is launched down the same fiber as the signal carrying light. This high power light is selectively coupled out of the core in the vicinity of each grating (if a sensor network is involved) and then absorbed by an energy conversion coating, which expands to distort the structure of the grating (and hence tuning the grating's response). By varying the intensity (power) of the high power laser light, the grating's response may also be altered, and thus is born the concept of active fiber sensing.

The motivation for the work presented herein is to expand on the concept of active fiber sensing by the successful demonstration of devices that utilize this new technology. Two functional sensors were demonstrated, the first being a discrete level sensor for liquid level monitoring and the second a vacuum sensor with a response similar to a Pirani gauge. Both sensors additionally have the capability for localized temperature sensing either via a single sensor or several when configured as a multipoint network. The level sensor improves on existing technology, surpassing many of the shortcomings of existing level detection while the vacuum sensor improves on existing MEMS technology by providing as good or better sensitivity while keeping with a simple, low cost design.

1.2 THESIS ORGANIZATION

Chapter 2 contains the background information necessary for the reader to gain an understanding of the operation and fabrication of a fiber Bragg grating. Basic device physics are covered along with typical transmission and reflection spectrums of the Bragg resonance wavelength. A brief description of the discovery of photosensitivity (and hence the Bragg grating) is given. A model for photosensitivity in optical fiber based on germanium oxygen deficiency centers (or so called 'wrong bonds') will be discussed, which is known as the color center model. A method of rendering standard fiber photosensitive, known as hydrogen loading, will then be covered. From here, the discussion will shift to techniques of fabrication. These include (but are not limited to) the internal writing technique, interferometric technique, point-by-point technique, and finally the phase mask technique.

Chapter 3 introduces fiber Bragg gratings as active sensors. This chapter covers, in detail, the modifications necessary to produce an active fiber Bragg grating, ready for sensing applications. The basic concept and operation of an AFBG is also covered. A comparison between AFBG level and vacuum sensors to existing MEMS and fiber-based technologies is also presented.

Chapter 4 includes material on the successful demonstration of AFBG based level and vacuum sensors. The discussion includes design, experimental setup, and results for each sensor.

Chapter 5 sums up all the material presented in this manuscript. A listing of publications resulting from this work is also given. A proposed plan for future work is discussed, dealing with the application of AFBGs for gas sensing.

2.0 BACKGROUND

In order to familiarize the reader with the operation and dynamics of active fiber sensing, it is first necessary to cover the basics of fiber Bragg gratings. The device physics will first be covered, followed by requirements that an optical fiber must possess in order to allow for the writing of a grating. Several methods of fabrication will also be discussed as well as applications of fiber Bragg gratings to passive fiber sensing.

2.1 DEVICE PHYSICS

In its most basic form, a Bragg grating is nothing more than a periodic modulation of the refractive index within the core of an optical fiber. This periodic index change may be further broken down by only considering two index changes spaced a distance L apart. Due to the difference in refractive index, light propagating through the core of the fiber will experience some reflection and transmission. This simple structure may be modeled after a device known as the Fabry-Perot etalon, which consists of two mirrors spaced a distance L apart. Only certain wavelengths are allowed to exist inside this optical cavity, being dictated by the following equation:

$$m\left(\frac{\lambda}{2}\right) = L \;\; where \;\; m = 1,2,3... \qquad (2.1.1)$$

with *m* being the mode number and λ being the wavelength of that mode. Bragg gratings can be thought of as a series of these etalon structures physically written into the core of the fiber [16-18].

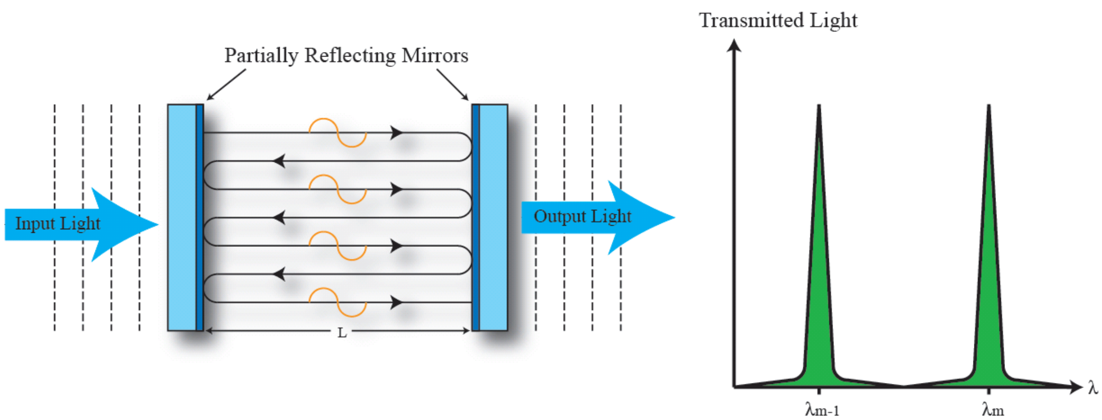

Figure 2.1.1 Illustration of the operation of a Fabry-Perot optical cavity. [17]

The etalon may be thought of as a type of optical 'band pass' filter, allowing only the tuned wavelength of light to pass through. This analogy can be further applied to that of Bragg gratings and the way in which they function (with a few subtle differences). Bragg gratings may also be thought of as an optical filter, with the exception of behaving like an optical 'notch' filter. The 'notch' in this filter is centered on a wavelength known as the Bragg resonance wavelength. The reflected spectrum will appear as it does for the light transmitted through an etalon. A typical reflection / transmission spectrum can be seen in Figure 2.1.2. It should be noted that this figure is provided to give the reader an idea of the appearance of the output from a typical grating. For telecom purposes, gratings are normally centered around 1.55μm. The above figure is somewhat outdated and can readily be seen from present-day spectrums. Grating quality has improved dramatically, with reflection spectrums having the same or nearly the same magnitude as the incoming light [17].

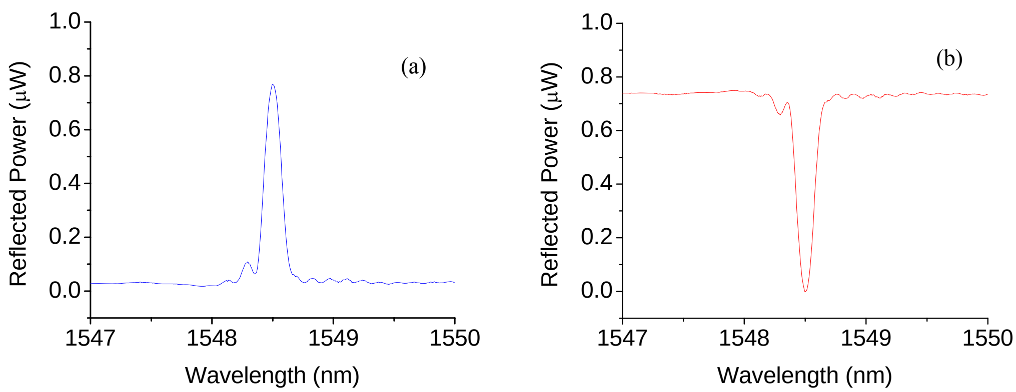

Figure 2.1.2 Illustration of a typical Bragg spectrum. Both reflection (a) and transmission (b) are shown.

Etalons can be applied as ‘tunable’ devices, where the length is changed to ‘scan’ the modes of the incoming light. If the output is fed into a detector and displayed on an oscilloscope, the result will look similar to the plot in Figure 2.1.2. Fiber Bragg gratings behave in much the same way, in that any stress or strain on the core causes minute changes in the spacing of the index changes thereby causing a shift in the reflected spectrum. This feature has been used widely in the area of fiber sensing and is the basis for the operation of active fiber Bragg gratings [17]. This will be discussed in greater detail in Chapter 3.0 .

2.2 PHOTO-SENSITIVITY IN OPTICAL FIBER

One cannot discuss Bragg gratings or their fabrication without first discussing photosensitivity in optical fiber. In order for a grating to be written into optical fiber, that fiber *must* be photosensitive. Since the discovery and use of optical fibers began, optical losses from absorption, waveguide imperfections, and Raleigh scattering have been extensively studied to improve the light-carrying efficiency of optical fiber [19]. In these studies it was discovered that germanosilicate fibers have a broad absorption peak at 240nm. This absorption is the cause for the discovery of the first self-induced gratings in 1978 by Hill *et al.* [1], since the second harmonic of the argon-ion laser light is close to the 240nm band. This second harmonic would have been present during the loss experiment conducted by Hill and co-workers, causing the observed index change and hence the discovery of the first Bragg grating. Lam and Garside (1981) later reported evidence that suggested a two-photon process was the cause of the induced refractive index change [20]. This effect however, went relatively unnoticed owing to the fact that this phenomenon was thought to only be present in the specialty small core fiber made by Bell Northern Research. Stone proved otherwise almost a decade later [21]. He showed that photosensitivity was present in many different fibers, all of which contained high concentrations of germanium.

Due to the fact that gratings fabricated using the self-induced method were limited to the argon ion wavelength of 488 nm, these gratings were not deemed useful for several reasons. It was found that slight tunability was attainable by applying axial strain to the fiber during fabrication. This however, did not render the grating usable in the infra-red region, which is commonly used in optical communication. In terms of fiber sensing, this type of grating structure does not inherently provide localized sensing information. Weak index changes due to the two photon process are responsible for the need to make very long gratings. Without the length, the magnitude of the index change (and hence the amount of detectable reflectivity) become difficult to detect. Finally, because these gratings are only operable in the blue-green wavelength region, they are susceptible to continuing evolution during their operation. While operating at or near the original writing wavelength of 488 nm, the harmonics responsible for the desired index change will still be present causing further development of the Bragg grating structure. In addition, if exposed to a different blue-green wavelength, the grating may become washed out and disappear all together. All of these factors make this type of grating unsuitable for communications use as well as localized sensing. The discovery of photo-induced refractive index change however, was one of several breakthroughs that helped develop the technology of fiber communication and sensing as it is known today.

In 1989, Meltz *et al.* [22] showed that strong index changes could be achieved simply by exposing the core of a germanosilicate fiber to ultraviolet light close to the absorption peak of a germania-related defect. This defect has a peak wavelength of absorption range around 240 nm, and is commonly referred to as a germanium-oxygen deficiency center (GODC). It has been shown to bleach when exposed to ultraviolet radiation [16]. Using the Kramer-Kronig relationship, Hand and Russel [23] developed a model to explain the refractive index changes by relating it to the absorption. In this model it was proposed that absorption caused the breaking of the GeO defect. The breaking this bond resulted in the creation of a GeE' center and the release of an electron. This electron is free to move about the glass matrix until trapped, either at the same site or another location within the molecule lattice [16]. (See Figure 2.2.1)

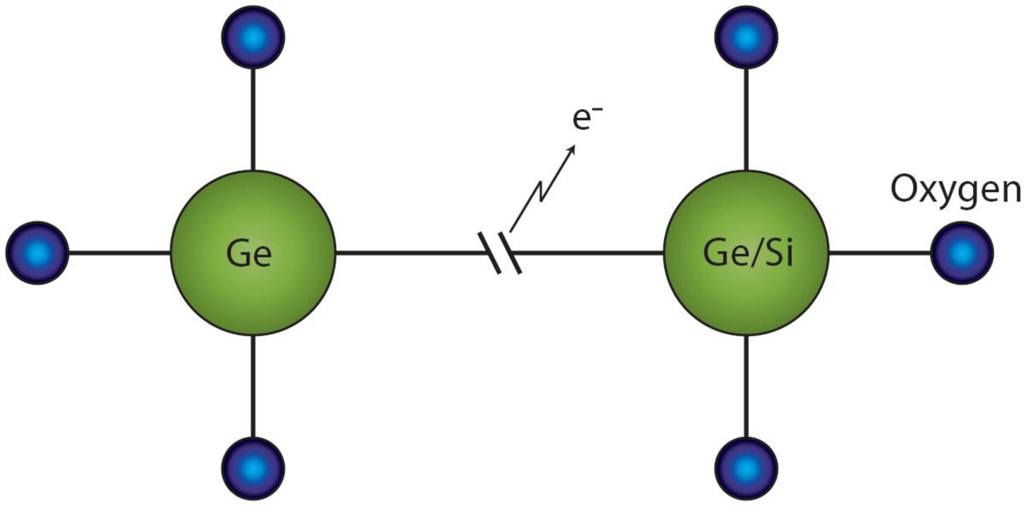

Figure 2.2.1 Germanium-oxygen deficiency center (GODC) defect thought to be the cause of photo-induced (photosensitive) effect observed in germania-doped silica fiber. Breaking of this bond releases an electron, which is then free to move about the lattice until captured again. [16]

This model is known as the color center model [16] due to the fact that point defects in the silica lattice exhibit strong absorption. Such point defects are caused by the fiber drawing process as well as ionizing radiation. Much research has been put into minimizing these defects to eliminate this absorption band; however their importance to Bragg gratings has changed their role significantly.

Part of the color center model has been experimentally found to support the idea that Ge-Si wrong bonds are responsible for the photosensitivity of germanosilicate fiber. These defect sites are also known as germanium-oxygen deficiency centers (GODC), as was mentioned earlier. By ultraviolet processing at 240 nm (the absorption band for these defects) the *wrong-bonds* are photoionzied, beginning the process responsible for refractive index change. (see Figure 2.2.2) As a result of the ionization process, an electron is released and a GeE' center is formed. This electron my immediately recombine with the GeE' center producing recombination luminescence or move through the lattice until it is trapped at a Ge(1) or Ge(2) center forming a $Ge(1)^-$ and $Ge(2)^-$ center respectively [16]. Ultraviolet absorption at these centers causes more defects to be created which in turn allows for more absorption. It is this creation of new defects that is responsible for the change in refractive index in the core of the fiber. It should be noted that this may not be the only mechanism responsible, just the most efficient found to date.

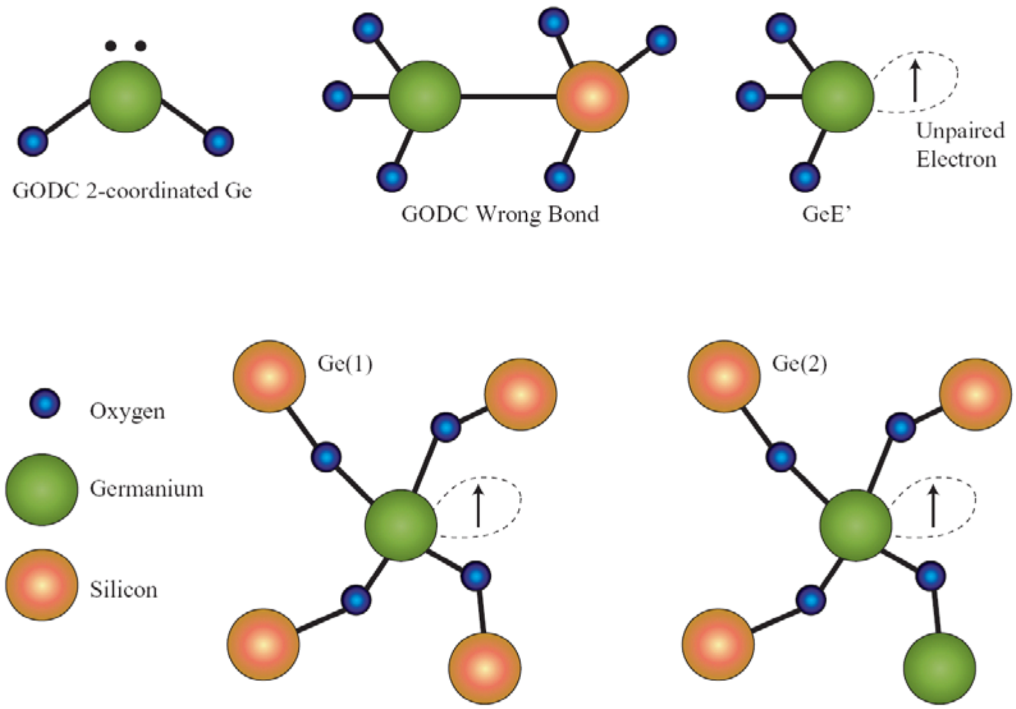

Figure 2.2.2 Illustration of possible GODC candidates. The Ge(1) and Ge(2) electron trap centers are shown along with the GeE' center. [16]

Photosensitivity in optical fiber can be defined as the amount of refractive index change for a given amount of UV radiation. Much work has gone into increasing photosensitivity in order to produce gratings with improved spectral response. One such method is known as hydrogen loading. With this method, fiber is exposed to high pressure (and often high temperature) hydrogen anywhere from a few hours to a few days. The hydrogen diffuses into the core of the fiber thereby increasing the photosensitivity. This method can produce index changes as high as 0.01, which is on the same order as the core / cladding index difference. Other methods of improving photosensitivity also include flame brushing and boron co-doping [16]. Flame brushing is similar to hydrogen loading, but the process time is on the order of hours instead of days. This method is fast, but tends to weaken the fiber. Boron co-doping must be implemented when the fiber pre-form is made. This method produces the highest photosensitivity, but requires one to have the availability to manufacture the fiber. Hydrogen loading is the most effective and simplest method and therefore is used the most.

Figure 2.2.3 shows the setup used to hydrogen-load SMF-28 fiber (and other non-photosensitive specialty optical fibers) to allow inscription of gratings. All gratings discussed in this manuscript where made photosensitive using this system. To make a fiber photosensitive, it is first loaded into the chamber at the far right. After the chamber connections are made tight, hydrogen is admitted into the chamber and brought up to a pressure of approximately 2500 psi. The chamber is then sealed off and left at pressure for approximately one week. At the end of the one week time period, the hydrogen is carefully vented out of the chamber into a fume hood. The chamber is then opened and the fiber removed. The now loaded fiber must be kept at -40˚C until immediately before inscribing. The low temperature slows the diffusion of hydrogen out of the silica lattice, allowing the fiber to be stored for several months while still retaining its photosensitive qualities. If left for too long, the fiber must he re-loaded for photosensitivity to be regained. Photosensitive fiber created in this fashion only has a working time of approximately 30 minutes, after which most of the hydrogen will have diffused out.

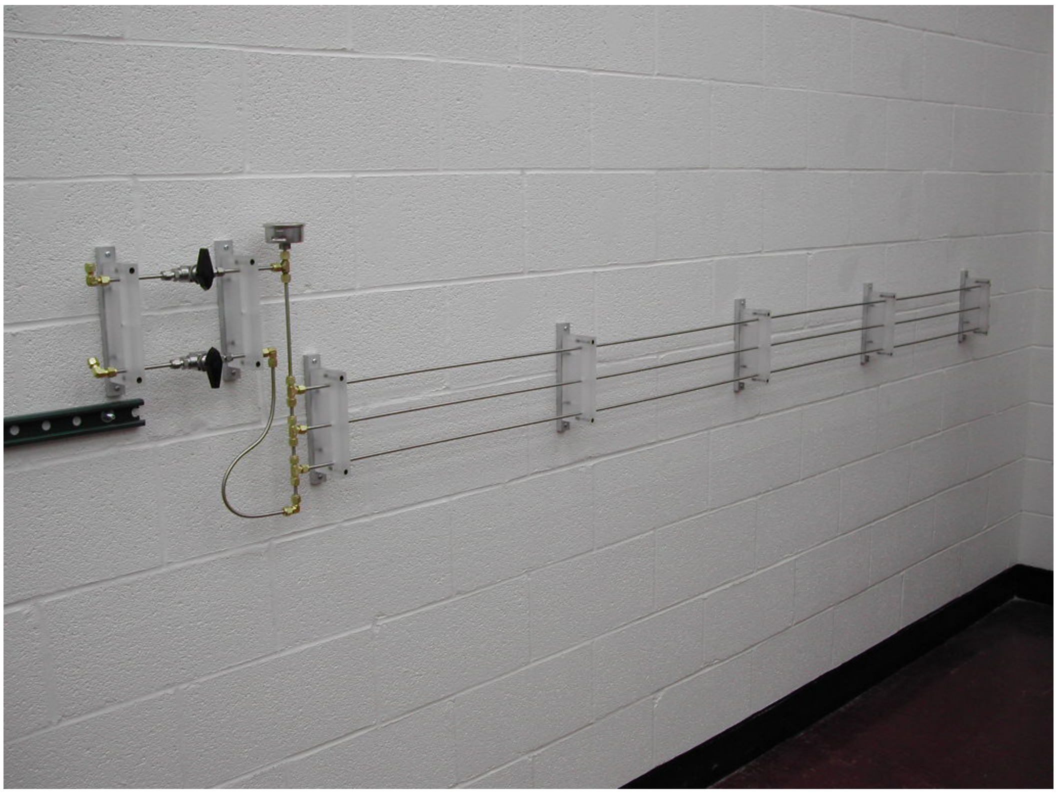

Figure 2.2.3 Hydrogen loading chamber located on the 7th floor of Benedum Hall.

2.3 FABRICATION TECHNIQUES

Bragg gratings were first discovered by Hill *et al.* [1] while conducting an experiment to study losses in a specialty germanosilicate optical fiber. In this setup, an argon-ion laser was focused into the core of the fiber using a 32x microscope objective. It was soon noticed that the output intensity from the opposing end of the fiber gradually decreased with time. Upon further examination, it was found that the reflected intensity had increased, so a setup similar to Figure 2.3.1 was constructed to further study this phenomenon. Periodic index changes were found to be responsible for the fiber behaving as a partially-reflecting distributed mirror.

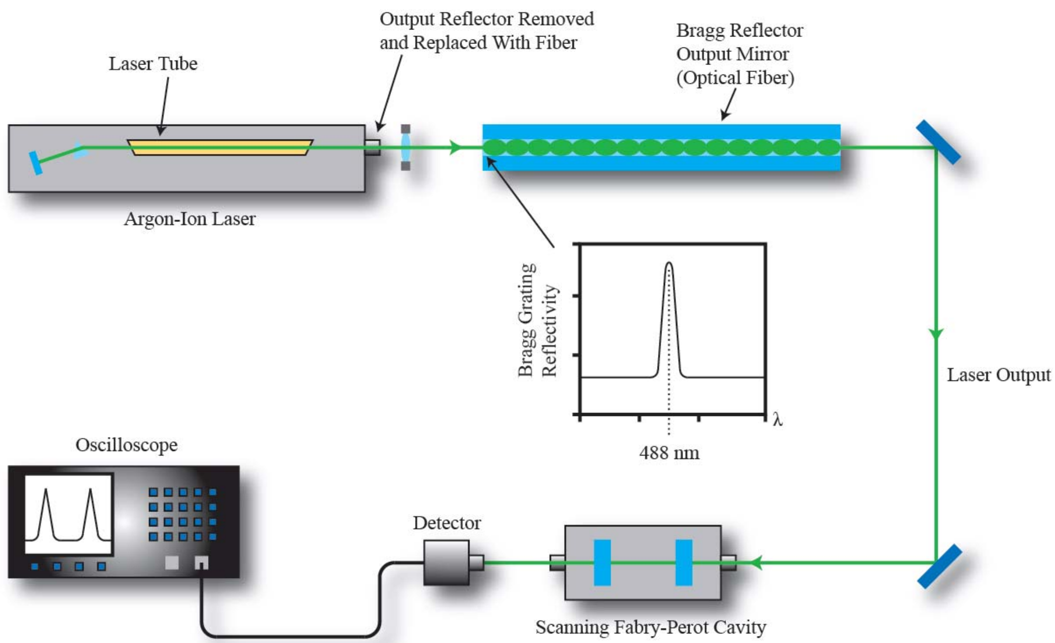

Figure 2.3.1 Experimental setup used to study losses in specialty optical fiber. Refractive index changes were induced due to a standing wave pattern set up in the core of the fiber. [1]

Due to the partial reflectivity at the cleaved ends of the fiber (approximately 4%), a weak standing wave pattern was set up inside the core of the fiber. Harmonics generated in this standing wave were close to the absorption wavelength of GODC defect sites (~240 nm) causing a periodic index change at the high intensity points. These changes in refractive index acted as a distributed reflector, coupling the forward traveling and reverse traveling light beams. This coupling provided positive feedback, which increased the intensity of the reverse traveling beam, which in turn increased the refractive index at the high intensity points. This process continued until the grating reflectivity became saturated. Gratings fabricated in this manner are referred to as self-organized or self-induced gratings [1, 16]. Grating fabrication will be discussed in greater detail in section 2.4.

The output objective of the laser was removed and the Bragg grating used as the output mirror. This was the first successful demonstration of stable CW oscillation of a distributed feedback laser (DFB). Since the Bragg grating is very wavelength selective, the output of the laser had a very narrow line width centered at 488nm (which coincidently was also the Bragg resonance wavelength) [1, 16].

Fabrication of Bragg gratings using this method is simple and the length of each grating is only limited by the coherence length of the light used for index modulation. However, gratings fabricated in this way are limited to the output wavelength of the argon-ion laser of 488 nm [1, 16]. Due to the fact that the index change for this type of grating is weak, the spectral width of the resulting grating is length-limited. For this reason, this type of grating is not well suited for sensing in small areas. Shorter gratings translate into sensing information about a smaller, local area. In addition, most telecom applications require gratings centered in the 1.55 μm range. For this reason, other methods of fabrication were explored so that the useful properties of Bragg gratings could be used at longer wavelengths.

It was later discovered by Meltz *et al.* [22] that optical fiber with high doping concentrations of germanium exhibited a strong absorption band located at 244 nm. This band is approximately 35 nm wide and coincides with the second harmonics of both propagating modes present in the output of any argon-ion laser. With the use of frequency doubling, it was possible to generate ultraviolet in the 240 nm range, which was in turn used to irradiate the core of the germanium doped fiber. Due to the absorption of ultraviolet light at 244 nm, an index change was induced in the fiber. Figure 2.3.2 illustrates the use of an interference pattern to generate the periodic modulation of the refractive index. The ultraviolet beam is split and then re-combined to generate the interference pattern. This method of grating fabrication is known as the interferometric technique [22]. Lenses were used to focus the beam down to a narrow line onto the core of the fiber. The resulting Bragg resonance wavelength is determined by the angle of the incoming beams:

$$\Lambda = \frac{n\lambda_w}{2\sin\varphi} \tag{2.3.1}$$

where λ_w is the ultraviolet wavelength, *n* is the effective index of the core, and φ is the half angle between the incoming beams [16, 22]. Since there is no restriction on the half angle (φ), varying the grating period by varying this angle is quite trivial. The inscription wavelength (λ_w) may also be changed, however this value is somewhat restricted by the absorption bands inherent in the fiber. Due to the fact that changing the angle is much easier, it is usually the preferred method.

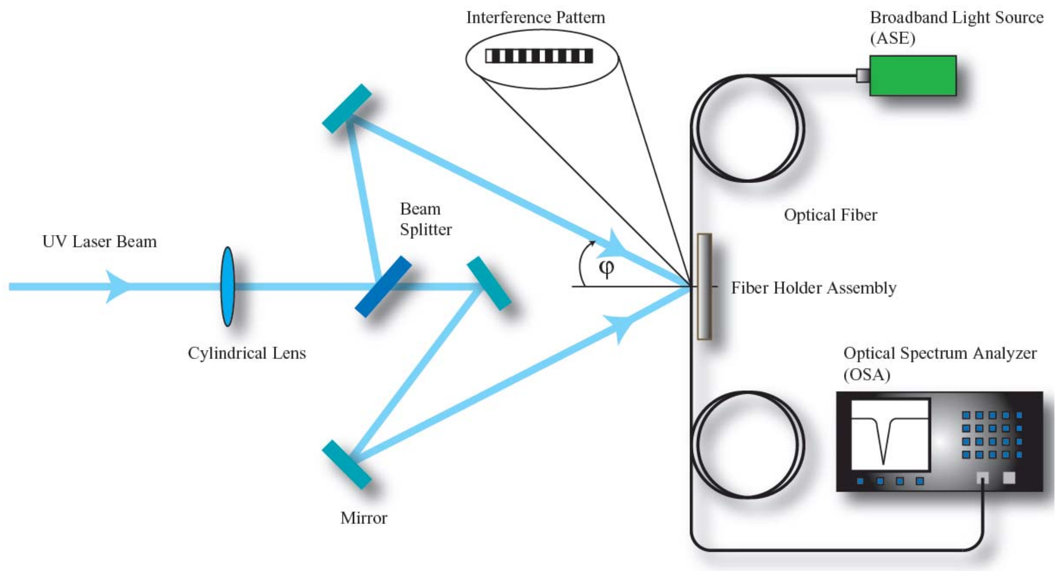

Figure 2.3.2 Interferometric fabrication technique using deep UV radiation. [16, 22]

This type of interferometer is known as an amplitude-splitting interferometric technique, since the incoming beam is split into two beams, each containing half the power of the original. These beams are later re-combined to form the fringe pattern needed for grating inscription. The main advantage of this writing method is that the wavelength of the Bragg grating may be easily selected, which allows for use in a variety of communications settings as well as active sensing. In addition, gratings of various lengths are also easily fabricated, thereby allowing selection of the spectral width of the grating response. Linearly chirped gratings may also be produced by the use of curved reflecting surfaces in the delivery path, thus allowing for complex grating structures to be fabricated using a simple setup.

The setup in Figure 2.3.2 however, is susceptible to mechanical vibration and changes in temperature. Even small (sub-micron) changes in the position of the various components will cause a shift in the fringe pattern, washing out the grating altogether. The laser light used must also be spatially and temporally coherent in order for the interference pattern to be generated properly. There are other variations to this type of grating fabrication that provide solutions to these problems, but they have limitations as well that make them undesirable due to complexity of the laser sources needed for spatial and temporal coherence [16, 18].

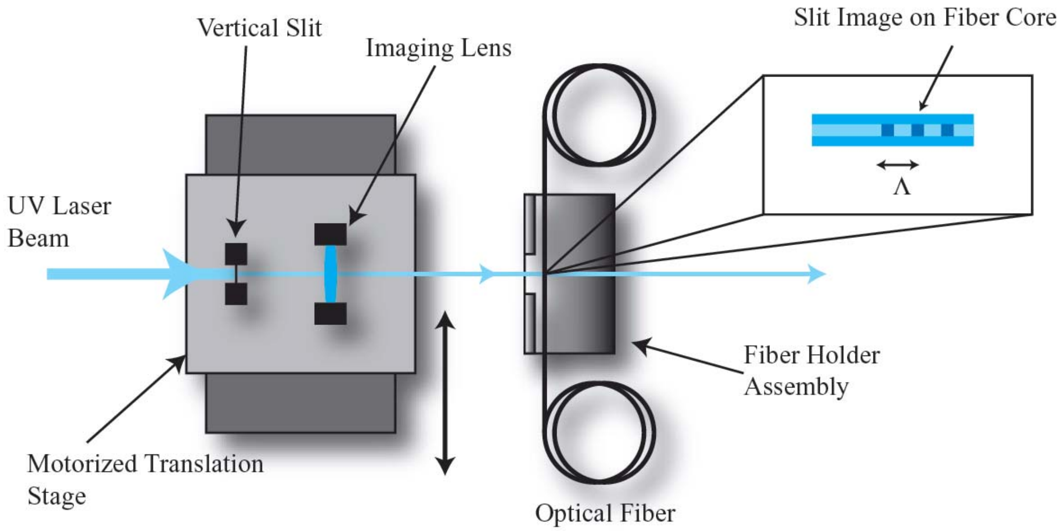

Figure 2.3.3 Point-by-point fabrication setup. [16, 18]

Another method that provides flexibility in making high-quality gratings is the point-by-point fabrication technique. In the setup shown in Figure 2.3.3, a single pulse of ultraviolet laser light is passed through a slit to shape the beam, which is then passed through a lens and focused onto the core of the fiber. Each pulse writes a single index change into the core of the fiber, which allows the Bragg grating to be built one index change at a time. The fiber is then advanced a distance Λ to maintain the proper period of the grating. At this point, the next index modulation is written. This process continues until the desired grating length is achieved [16, 18].

The major advantage to this setup is that it allows for precise incorporation of desired grating parameters into the fabrication process. Since the period of the grating can be modified by changing the amount of translation, variations in grating length, period, and spectral response are easily attainable. The magnitude of the index change can also be changed by changing the magnitude of the ultraviolet pulse. There are however, limitations to this method. Because gratings are sensitive to thermal effects, variations in period due to temperature or strain can cause errors in the fabrication process. For this reason, gratings fabricated with this method are often very short. Also, because of the submicron translation and tight focusing of the ultraviolet beam, gratings that are useable at 1550 nm have yet to be successfully fabricated. The period required for a grating at this wavelength is on the order of 530 nm [16, 18].

The most effective method for fabrication of Bragg gratings is known as the phase mask technique. This technique involves the use of a diffractive element (a phase mask) to generate the interference pattern required for grating fabrication. Phase masks are fabricated by either holography or electron beam lithography. Holographically fabricated phase masks have the advantage of having no stitch error, however e-beam lithography allows for complex patterns to be etched into the mask. These patterns are a one dimensional surface relief structure built in high quality fused silica slides, which are transparent to the ultraviolet beam. These masks are constructed so that the zero order diffracted beam is suppressed to less than a few percent, while the diffracted plus and minus first order beams are maximized so that each contains approximately 35% of the initial incident power. Close to the phase mask, a near field fringe pattern is produced by the first order diffracted beams. The period of this fringe pattern is one half the period of the phase mask. This pattern then induces index changes when focused onto the core of the fiber, which is placed immediately behind the phase mask. An illustration of this setup can be seen in Figure 2.3.4 [16, 18].

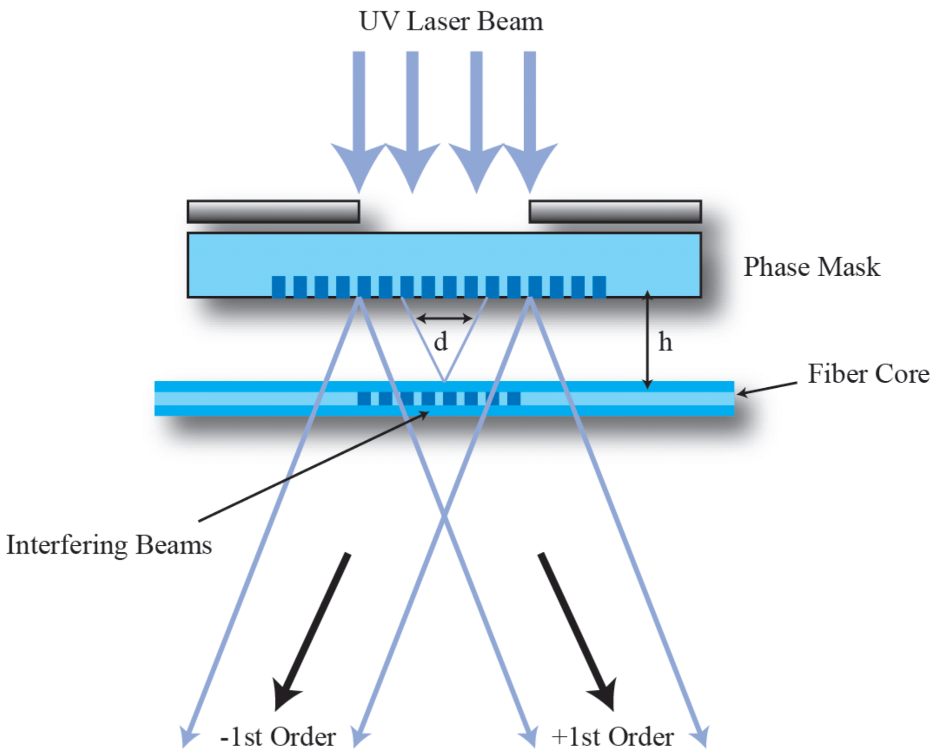

Figure 2.3.4 Setup of the phase-mask fabrication technique. [16, 18]

Figure 2.3.5 and Figure 2.3.6 show the phase mask setup that was used to fabricate all of the fiber Bragg gratings discussed in the experimental section of this manuscript. The process of grating fabrication is as follows: A camera is first used to align the fiber to the phase mask. The fiber must be as close to parallel with the mask as possible by visual inspection. At this point it is advanced to be as close to the phase mask as possible without physically touching. If the fiber comes in contact with the mask, the holographic diffraction pattern on the mask may become damaged causing defects in grating fabrication, and possibly the need to purchase a new phase mask. Figure 2.3.5 illustrates this setup, showing both the phase mask and fiber during the process of writing. Figure 2.3.6 illustrates the diffraction pattern that is present when the setup is properly aligned. The appearance of this diffraction pattern is a good visual indicator that everything is in the right place. If these patterns do not appear, the grating will not form well or at all.

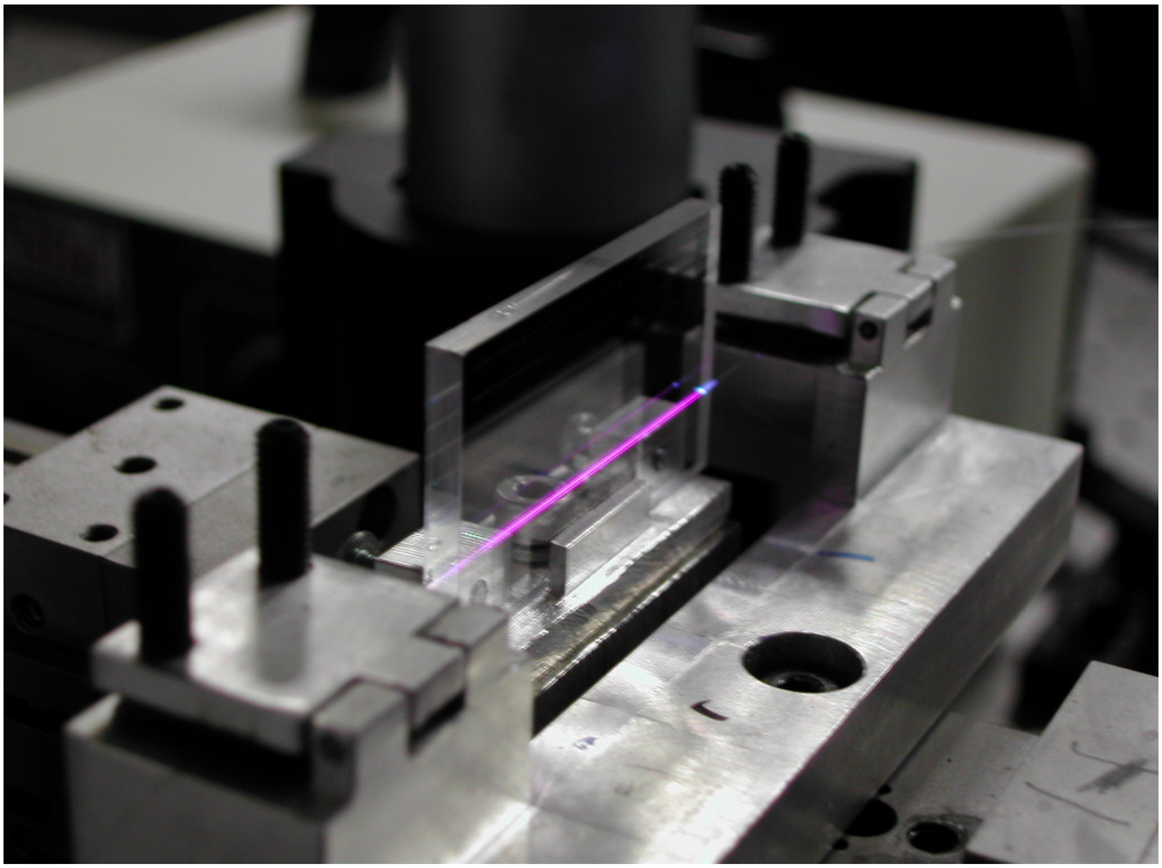

Figure 2.3.5 Setup showing a Bragg grating during the writing process.

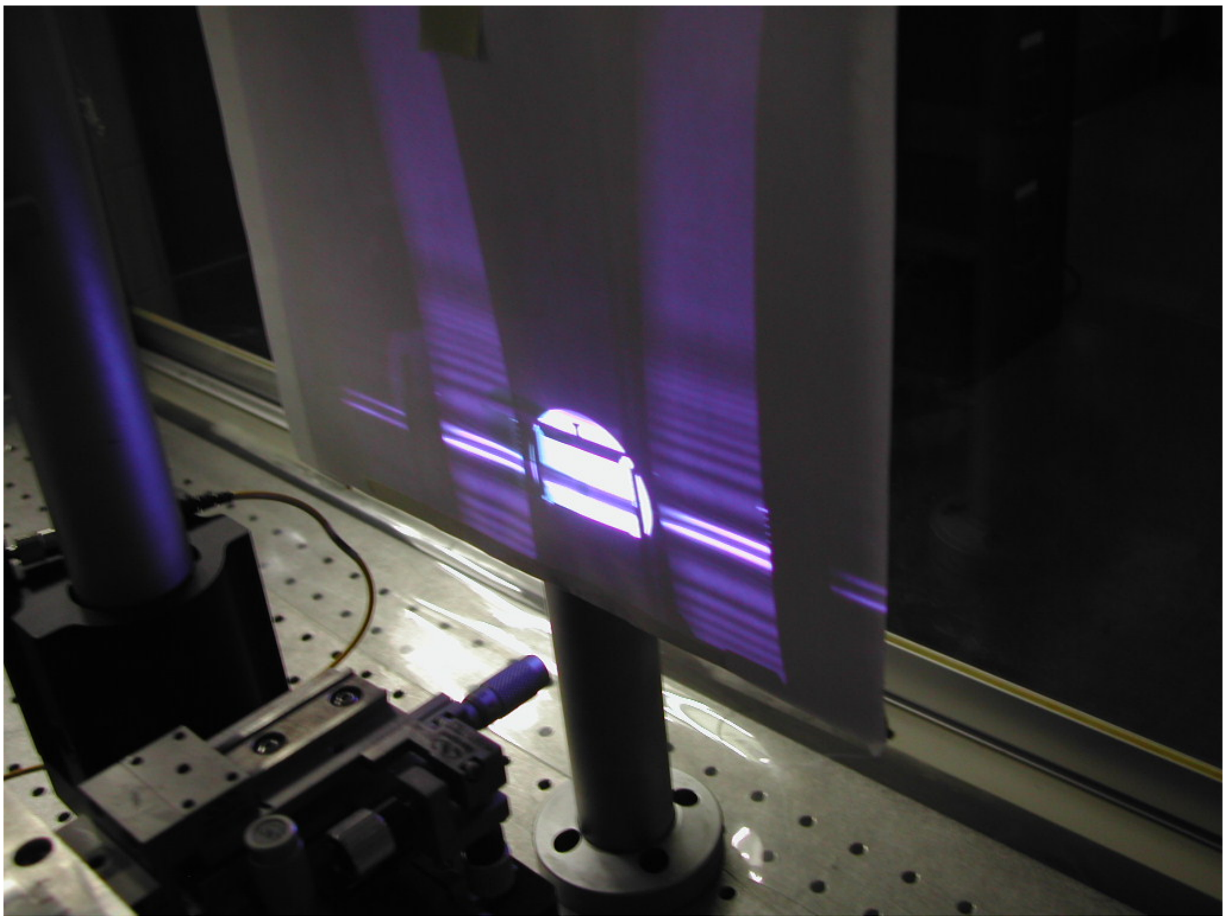

Figure 2.3.6 Diffraction pattern seen when the phase mask and fiber are properly aligned.

2.4 GRATINGS AS PASSIVE SENSORS

The making of fiber Bragg gratings is only one step along the way to active fiber sensing. The operation of these devices as passive sensors must first be understood before moving on to the active sensor design. This section aims to give the reader an overview of the dependence between spectral response of a Bragg grating and environmental factors such as temperature, stress, strain, and pressure. In addition, several types of Bragg grating structures will also be covered along with their application to passive sensing.

Along with the discovery of fiber Bragg gratings, Hill *et al*. [1] was also the first do demonstrate the dependence of both the fabrication and operation of a Bragg reflector on environmental factors such as temperature and strain. During operation, the spectral response of a grating may be changed by the application of axial strain (tension) or by varying the temperature of the surrounding medium, which in turn heats (or cools) the fiber. Both of these factors cause minute changes in the spacing of the periodic perturbation in the grating, thereby causing the resonance wavelength to change. In its most basic form, the Bragg reflector can serve as a sensor for monitoring both ambient temperature of a surrounding medium and any stress or strain induced by applied tension, pressure, or other deformation of the fiber. This is the basic building block for the concept of active fiber sensing.

Hill based his sensitivity observations on the following equation, which describes the temperature and stress dependence of the Bragg reflector response:

$$\Delta\lambda_B = 2\left(\Lambda\frac{\partial n_{eff}}{\partial l} + n_{eff}\frac{\partial\Lambda}{\partial l}\right)\Delta l + 2\left(\Lambda\frac{\partial n_{eff}}{\partial T} + n_{eff}\frac{\partial\Lambda}{\partial T}\right)\Delta T \qquad (2.4.1)$$

The value $\Delta\lambda_B$ is the change in resonance wavelength of the grating due to an applied temperature or change in axial length of the fiber, were Λ is the spacing of the periodic perturbation in the core of the fiber, and n_{eff} is the effective refractive index. The first term in

(2.4.1) is representative of the effect of an applied strain on a Bragg grating. This strain causes a change in the spacing of the grating structure and a strain-optic induced change in the refractive index. This strain effect may be represented as:

$$\Delta\lambda_B = \lambda_B\left(1 - p_e\right)\varepsilon_z \tag{2.4.2}$$

The term ε_z is the applied strain along the axis of the fiber in $\mu\varepsilon$, with p_e being the effective strain-optic constant, which is defined as:

$$p_e = \frac{n_{eff}^2}{2}\left[p_{12} - \upsilon\left(p_{11} + p_{12}\right)\right] \tag{2.4.3}$$

In this equation, υ is Poisson's ratio, with p_{11} and p_{12} being components of the strain optic tensor. Using values for a typical germanosilicate fiber of $p_{11} = 0.113$, $p_{12} = 0.252$, $\upsilon = 0.16$, and $n_{eff} = 1.482$, the resulting expected strain sensitivity at around 1550 nm is 1.2 pm shift in resonance wavelength per 1 με of applied strain [16, 18].

The second term in (2.4.1) is representative of the effect of temperature on the spectral response of a Bragg grating. A resonance shift in this case is due to a change in grating spacing from the effects of thermal expansion of the optical fiber as well as changes in the index of refraction. This thermal term may be re-written as:

$$\Delta\lambda_B = \lambda_B\left(\alpha_\Lambda + \alpha_n\right)\Delta T \tag{2.4.4}$$

The value of $\alpha_\Lambda = \left(1/\Lambda\right)\left(\partial\lambda/\partial T\right)$ is the thermal expansion coefficient of the optical fiber, or 0.55×10^{-6} for silica. The second term $\alpha_n = \left(1/n_{eff}\right)\left(\partial n_{eff}/\partial T\right)$ is the thermo-optic coefficient, which for Germania-doped silica core fiber is approximately 8.6×10^{-6}. Using these values, the expected resonance wavelength shift for a 1550 nm grating is approximately 13.7 pm/°C [18].

From these equations, it is easy to see the dependence of the resonance wavelength response of the Bragg grating on both temperature and strain. For these reasons, Bragg gratings are quite useful as passive sensors for structural monitoring, where the gratings may be multiplexed into one fiber, allowing multi-point sensing information to be monitored. It should be noted that, if only one environmental factor is desired to be measured (either temperature or strain), the other measurement must be accounted for so as to not introduce error into the measurement.

As passive sensors, Bragg gratings have found much use in the telecom industry. This usefulness arises from the several variations of grating structures that may be fabricated with almost all of the previously mentioned fabrication techniques. The first of these (and the most basic) is that of the common Bragg reflector. An illustration of this structure may be seen in Figure 2.4.1. An example of a typical transmission spectrum is also shown.

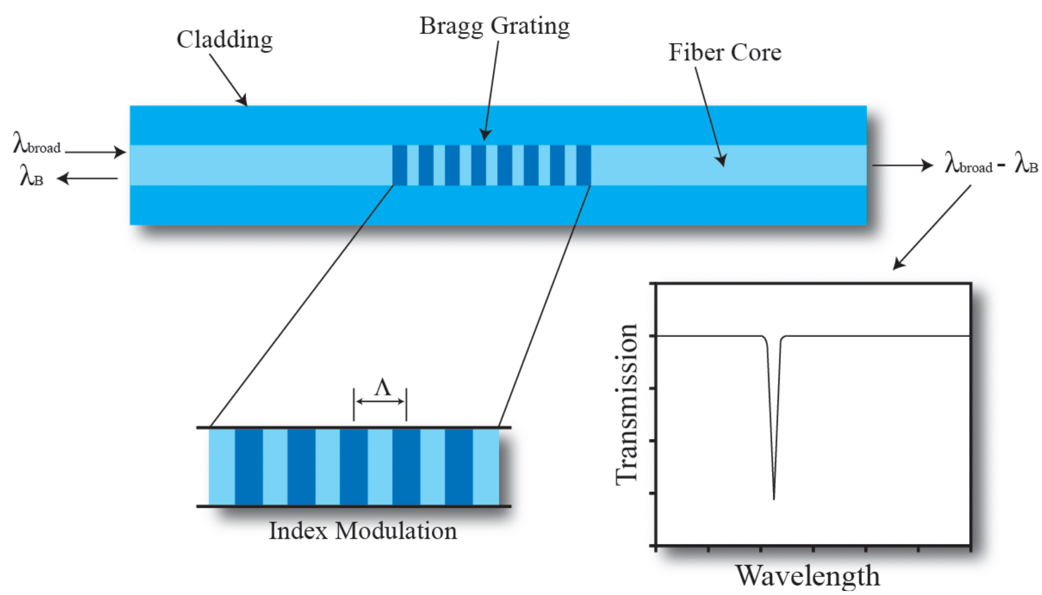

Figure 2.4.1 Illustration of a common Bragg reflector. [16, 18]

This grating was the first grating to be fabricated using the self-induced method described previously by Hill *et al*. [1]. The index modulation is written in the core so that it lies perpendicular to the axis of the fiber. This type of grating can function as a narrow band mirror, or notch filter (when used as a transmission grating). When combined with other Bragg structures, it can also function as a band-pass filter. The Bragg resonance wavelength can be found by the following equation:

$$\lambda_B = 2n_{eff}\Lambda \tag{2.4.5}$$

Where λ_B is the free space Bragg resonance wavelength of the light that will be back reflected down the fiber, n_{eff} is the effective refractive index of the fiber core at the resonance wavelength, and Λ is the period of the Bragg grating. Common Bragg reflectors were used for all experiments discussed in this manuscript.

The second type of Bragg structure is known as a blazed or tilted grating. By tilting index perturbations with respect to the fiber axis an optical tap may be fabricated. A typical blazed grating structure may be seen in Figure 2.4.2.

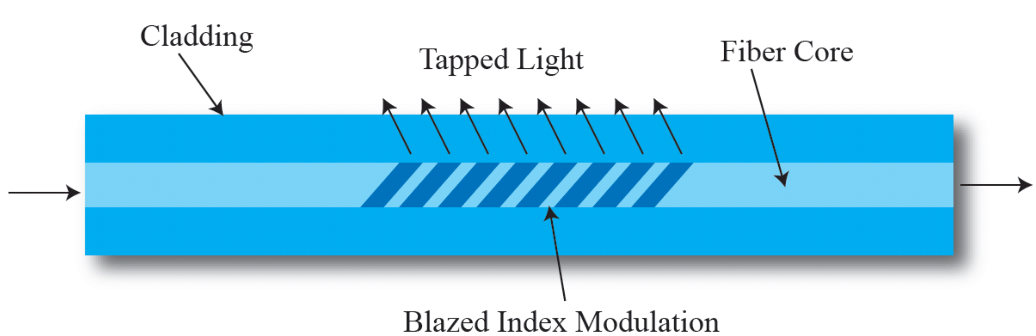

Figure 2.4.2 Illustration of a blazed Bragg grating. [16, 18]

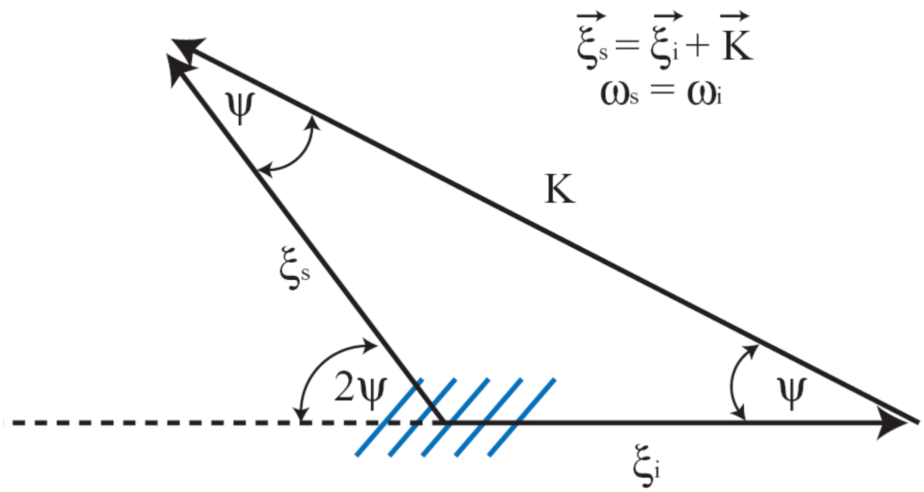

Figure 2.4.3 Vector diagram of a blazed grating. [16, 18]

Due to the tilted index modulation, light that is otherwise guided back down the fiber is now coupled into the cladding and out of the fiber into the surrounding air. The strength of the index change and the angle of the grating determines the coupling efficiency and bandwidth of the light that is tapped out of the incoming beam. This type of grating is useful in the telecom industry when frequency division wavelength multiplexing (FDWM) is used for communication. This communication scheme uses several channels centered at several wavelengths. Individual channels may be selected and tapped out of the fiber through the use of the blazed structure. This is especially useful since it does not require that the fiber be broken (which can introduce further loss) and is a simple solution for channel selection. The criterion that satisfies the Bragg condition of a blazed grating is similar to a common Bragg reflector. A vector diagram of the blazed grating Bragg condition may be seen in Figure 2.4.3. The wave vector of the grating is at an incident angle Ψ with respect to the fiber axis. The magnitudes of the scattered and incident wave (ξ_s and ξ_i respectively) must be equal. Through simple trigonometry analysis, it can be shown that the scattered wave vector must be at an angle 2Ψ with respect to the fiber axis. By applying the law of cosines to the above diagram, it can also be shown that:

$$\xi_i^2 + \xi_s^2 - 2\xi_i\xi_s \cos\left(\pi - 2\Psi\right) = K^2 \tag{2.4.6}$$

which reduces to:

$$\cos\left(\Psi\right) = \frac{K}{2\xi} \tag{2.4.7}$$

This shows that the scattering angle is restricted by the Bragg wavelength and the effective index of refraction. Note that from the first equation, it is clear that for this type of grating structure, different wavelengths emerge at different angles, as well as different modes for each of those wavelengths due to their different propagation constants. This makes the blazed grating very versatile for communications signal recovery. In a low cost Bragg grating array for environmental monitoring, this type of grating may be used to passively select responses from individual sensors in the network. The selected signal tapped out of the fiber can then be monitored with a simple photodiode [16, 18].

The last grating structure is that of the chirped Bragg grating. This type of grating is fabricated by changing the angle of the fiber with respect to the phase mask during writing. By changing this angle, the period of the grating is gradually increased as the fiber gets further from the mask. It should be noted that other methods of fabrication besides the phase mask technique may be used; however this is the easiest method. This 'chirped' structure is illustrated in Figure 2.4.4a. This is known as a linear chirped grating. Figure 2.4.4b illustrates the approximation of a liner chirped grating by the use of a step approximation. With step approximation, the linear variation in the grating period is approximated with several gratings with successively increasing period. This method can be used to successfully repeat grating fabrication without having to worry about the angle of the fiber with respect to the diffraction pattern, making fabrication much easier and more readily repeatable [16, 18].

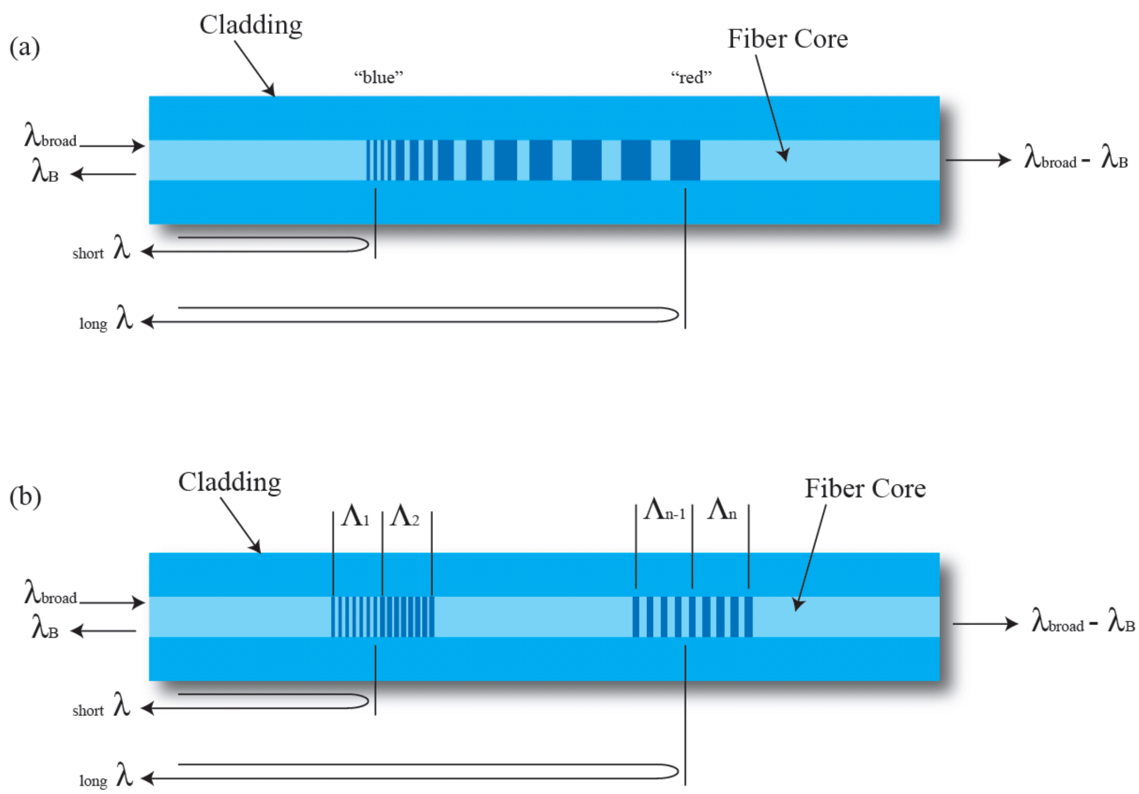

Figure 2.4.4 Structure of a chirped Bragg grating (a). Approximation of a linear chirp with stepped period change (b).[16, 18]

Chirped gratings are useful when dealing with optical amplifiers in high-bit rate, long haul communication systems. In these systems, the distance over which they can transmit is limited by pulse broadening caused my chromatic dispersion. This dispersion can be eliminated by a device which has a dispersion equal but opposite in sign to that of the fiber link. In chirped gratings, the Bragg resonant frequency is a linear function of the position along the axis of the fiber. Different frequencies present in the pulse are reflected at different points, which then introduce different delay times. These gratings are useful as dispersion compensators to compress temporally broadened pulses [16, 18]. In the area of fiber sensing, large fiber networks may need signal dispersion compensation when the number of sensors on the network becomes large.

3.0 FIBER BRAGG GRATINGS AS ACTIVE SENSORS

Fiber Bragg gratings are key components for communication and optical sensing as these in-fiber sending components offer several advantages over other electronic and optical devices [1]. These advantages include high sensitivity, long lifetime, immunity to electromagnetic fields, and superior performance in harsh environments. Though these devices are purely optical and appear like the logical choice over traditional components, they are limited by their total passivity. Sensor elements of a passive nature do not allow for active adjustment of sensor parameters to adapt to a changing environment. Over the past several years, intensive research has been carried out with the intent of developing a tunable fiber-Bragg grating, thereby enhancing the functionality of a purely optical device. Various tuning methods have been developed including mechanical actuation [10], piezo-electric actuation [11], electrowhetting [12], and on fiber-electrical heating [13-15]. Despite these advances in tuning capabilities, active fiber components still posses a common drawback. For every active-fiber component, three things are still required: an energy source, a mechanism to deliver this energy, and an on-fiber mechanical means to tune the device. Electrical energy has been the only energy used to date, requiring that an electrical cable be run along with the fiber to power an in-fiber device. This additional cabling leads to increase in manufacturing cost from both material and the need to shield from electromagnet interference, as well as concerns with lifetime due to delicate packaging. There is also the problem of having on-fiber contacts, which are often difficult to fabricate, leading to even further costs. Due to these additional costs, such fiber components would no longer be economical for use in hostile environments. The advances listed above often overshadow the appeal of a purely-based optical component when the improvements are weighed against the cost.

3.1 CONCEPT AND ADVANTAGES

As was mentioned before, the applications of fiber-Bragg gratings are limited by the fact that they are passive sensors. This type of sensor is a good choice for an otherwise ‘static’ environment, where conditions (i.e. thermal variations, pressure, etc) remain constant. Since the ideal ‘static’ environment is rarely encountered in sensing applications, a sensor must possess the ability to adapt (or be ‘tuned’) to the changing conditions. Passive gratings are fabricated with specific parameters, which are not conducive to modification during operation unless basic enhancements to the fiber structure are made. These modifications allow for the changing of the grating structure, thereby allowing a shift in the center wavelength. This type of ‘tuning on the fly’ gives this type of modified grating the name of the active fiber sensor.

Several approaches [10-15] have been demonstrated to allow for tuning of a passive Bragg grating, in both sensing and filtering applications. All of these techniques employ the use of the application of axial strain to the grating structure through some external means, thus changing the fundamental period of the grating and causing a detectable center wavelength shift.

Figure 3.1.1 illustrates the modification needed to allow for a passive sensor to be actively tuned. All gratings discussed in this manuscript were fabricated using the phase mask technique, which requires that the acralyte fiber jacket be removed prior to grating inscription. This is a vital step in making an active fiber sensor. Though the fiber is weakened in the area around the grating, the cladding is exposed for addition of a thin metallic coating, which is plated onto the fiber. It is this coating that is responsible for the tunability of an active fiber sensor.

During operation, two optical signals are transmitted down the fiber to the grating. One signal, composed of mostly broadband IR, is used as an interrogation signal so that the spectral response of the grating may be obtained. This response is indicative of the sensor’s surroundings such as temperature, strain, and pressure. The second signal provides power to the sensor by supplying high power laser light to the grating, typically on the order of a few hundred milliwatts. This high power laser light is supplied to the grating via a multimode fiber. Due to the fact that most gratings are fabricated in single mode fiber designed for 1550 nm, propagation of the high power laser light is not possible since the wavelengths used in experiments discussed herein are on the order of 515 – 910 nm. To overcome this difficulty, the single mode fiber is cut

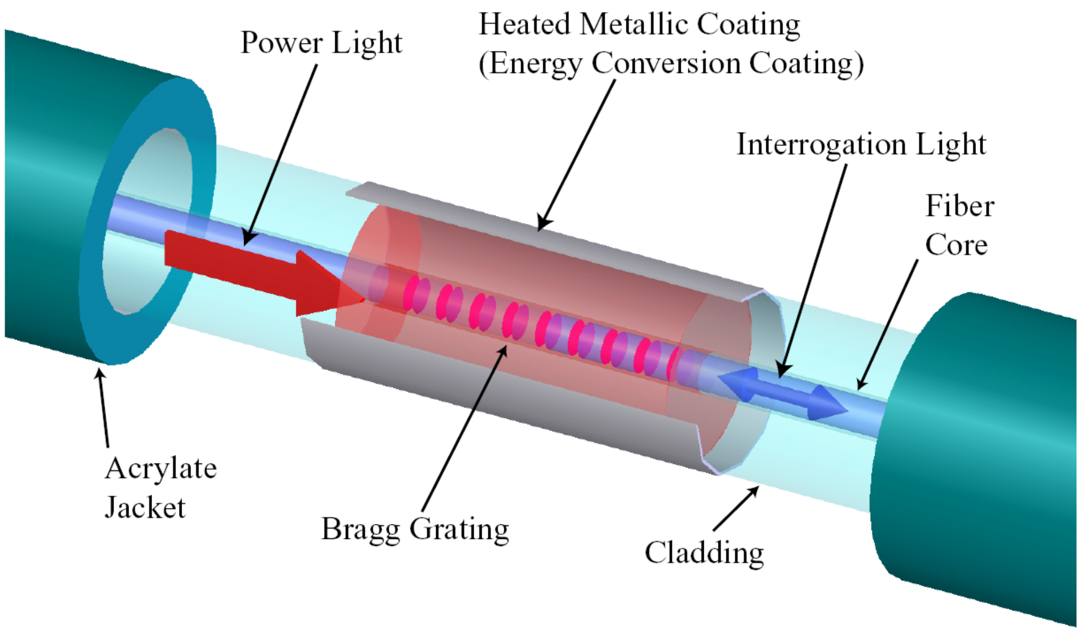

Figure 3.1.1 Illustration of the operation of an active fiber sensor.

as close to the grating as possible (within 1 cm) and fused to the broadband fiber. Though this adds another weak point to the fiber, the splice junction plays a key role in the operation of the sensor. There is a relatively high mode mismatch between the broadband and the single mode fiber, which causes the high power laser light to couple into the cladding of the single mode fiber. This laser light gradually leaks out of the fiber with increasing distance from the splice junction. As the light leaks out, it is absorbed by the metallic coating, which is why it is important to keep the splice junction as close to the Bragg grating as possible. For all sensors discussed here, this coating was silver, which has a much higher coefficient of expansion (5.5 x 10^{-6}K) than that of silica (0.66 x 10^{-6} K). The expanding film causes axial strain on the fiber Bragg grating distorting the period and thereby causing a change in the sensor's spectral response.

Now that the basic operation of actively tuning a fiber Bragg grating is understood, it is important to discuss the various ways in which this may be employed in a sensing environment. The setup illustrated in Figure 3.1.1 may be tuned in two ways. The first tuning method was just previously discussed. The second variable that affects tuning involves the surroundings of the sensor. Environmental factors such as the presence of liquid or air flow will greatly change the thermal response of the metallic coating. For this reason, this method of wavelength tuning has found much success in the area of fiber sensing.

One may question why this method is advantageous compared to other techniques. This is quite simply explained when this technique is demonstrated with the use of only a single fiber feed through. This is desirable in environments where leaks of volatile liquids (fuel tanks) or sustainable atmospheres (the inside of a space shuttle) are a concern. Traditional sensing technologies employ the use of many wire feedthroughs, which allow for the potential of increased risk of failure (or leak) at the site of entry or exit of the signal and control lines. When dealing with many sensors over a very long distance, one must also consider the effects of electromagnetic interference. This is quite often a problem and can cause erroneous errors in sensor output readings. In addition, a Bragg grating-based sensor employing the active tuning technique proposed here is not application specific and may be applied to many sensing applications with no modifications. Various other tuning techniques that have been proposed to actively tune fiber Bragg gratings are described below:

- **Mechanical Actuation [10]**

  This method employs the use of a flexible beam to apply axial compressive strain to the fiber, thereby distorting the grating period and causing a center wavelength shift. This method is advantageous since it provides a broad tuning range (90 nm) and a stable set-and-forget tuning capability. Despite this broad range, tuning is achieved through the use of a mechanical motor and micrometer assembly. Response time of this system is slow when compared to that of the AFBG and will have a higher overhead cost associated with fabrication of the sensor. Since this tuning method was designed for a communication type application, it is not well suited for fiber sensing. In addition, temperature stability due to the large thermal mass of the frame and bending substrate may be a concern. The increased part count, higher cost associated with packaging and complexity, and in-ability to be applied to multiple sensing applications make this method a poor choice for a broad range of sensing applications including multiple point sensor networks and sensing in harsh environments.

- **Piezoelectric Actuation [11]**

  This method employs a piezoelectric coating plated onto the outer surface of a bare fiber surrounding an FBG as well as an on-fiber resistive heater to achieve resonant wavelength tuning. While this method is a step in the right direction toward AFBGs, it still has a higher associated cost due to the support hardware required to operate the device. In addition, electrical contacts made to the coating will be fragile making packaging difficult. For this reason, this sensor may not be suitable for harsh environments, particularly in applications where large temperature fluctuations and high G forces are sustained.

- **Thin Film Heaters [13-15]**

  Thin film on-fiber heaters strive to achieve tunability by exertion of a tensile strain along the axial direction of the fiber during thermal expansion of the coating. This method is quite effective since the thermal expansion of the coating is chosen to be greater than that of the silica on which it is coated. Applications range from variation of chirp in LPGs by using a tapered film whereas the same heater may be used to control the position of a fluid plug inside a micro-structured fiber to achieve the same effect. This method is closer still to that of an AFBG, but again, the same pitfalls are still present. Slower response time, difficulty in packaging due to fragile nature of contacts, higher cost from additional support hardware and fabrication, and susceptibility to electromagnetic interference are still problems to be dealt with when considering this type of tuning method.

All of the methods described here are not suitable for simple, single feed through fiber networks. These methods were designed for filtering applications in communications, so their use in sensing environments does not bode well for the criteria required of a sensor in these types of applications. In addition, their design complexity and difficulty in packaging would most likely make them cost-prohibitive when compared to an AFBG. The reader should now recognize the versatility that is provided by an AFBGs ability to be applied in many sensing applications as well as telecommunications filtering. Various applications of active fiber Bragg grating technology will be discussed further in Chapter 4.

The reader should note that the operation described previously claims a single fiber feed through. For simplicity during experimentation, interrogation light and power light were supplied from opposite ends of the fiber, which would lead one to suppose that two feedthroughs would be needed for an application. This however, is not the case. Through the use of double-clad fiber, both power light and signal light may be carried on the same fiber through the use of a power combiner. The second cladding on double-clad fiber is of the proper diameter to confine the propagation modes of the power laser light, thus allowing power delivery to the Bragg grating. Upon reaching the grating, some of the light will be coupled out into the outermost cladding and the sensor will operate as described earlier.

3.2 THERMAL BASED LEVEL SENSOR

In today's age of industry, liquids are a common commodity when it comes to manufacturing. These liquids may often be thought of as the life-blood that helps a wide array of products come to be. In order to keep up with demand, an adequate supply of these liquids must always be on hand. For this reason, liquid level measurement has become an interest in nearly all commercial and scientific fields. Various reasons have arisen for this, from reducing emissions of volatile organic chemicals (VOC) due to opening of tanks at petroleum plants to gauging the amount of cryogenic fuel on spacecraft. Various blends of sensor technology have been developed for this broad range of applications, including non-contact level sensing using computer vision [24], acoustic resonance [25], and radar [26]. This section aims to cover fiber-based devices and compare them to AFBG technology so that the reader may see the inherent advantages of using this new technology over existing implementations of liquid level sensing. In addition, an implementation using diode point-sensors will also be reviewed, showing the inherent advantages of the AFBG when used in an array configuration.

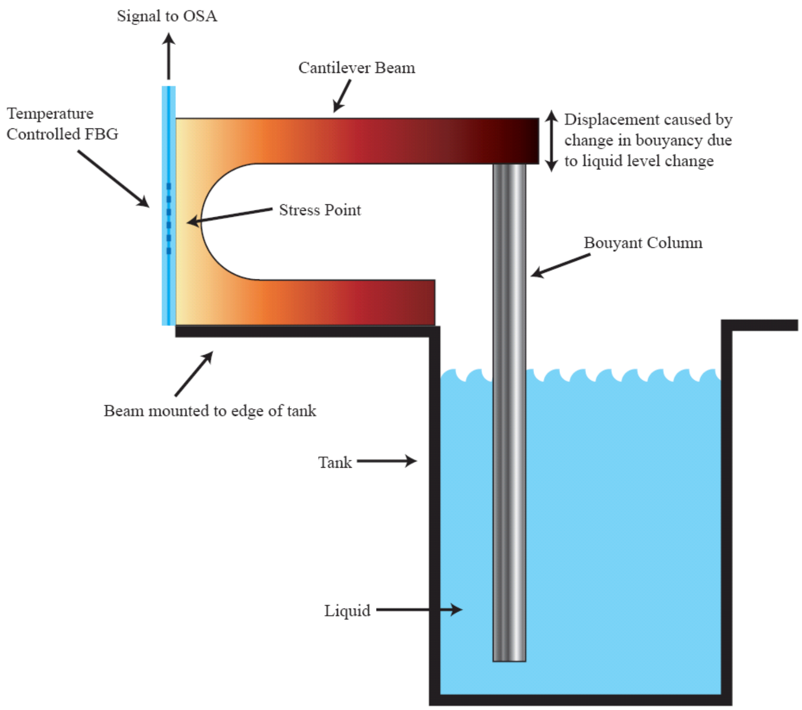

Figure 3.2.1 Illustration of bending beam cantilever setup for liquid level sensing. [27]

Figure 3.2.1 illustrates the first implementation of liquid level sensing that employs a Bragg grating as the primary sensing element proposed by Guo *et al.* [27]. In this setup, a Bragg grating is placed along the back of the cantilever beam and adhered to the surface. Any force applied to the end of the beam will induce an axial strain on the fiber, causing a shift in the spectrum and broadening of the peak. Stress is applied to the beam via an appropriately sized buoy (or float) attached to the end. Force arises from the amount of liquid in the vessel, which determines the amount of buoyancy that will be experienced by the float. To measure liquid level, the reflection strength and peak width (FWHM) are monitored to determine liquid levels. Since axial strain is applied along one edge of the grating, chirping occurs causing the reflection peak to broaden as well as a reduction in peak strength. Due to this type of operation, this sensor is immune to temperature variations, which only incur a shift in the location of the center wavelength of the grating and do not affect the shape of the response.

Though this sensor is simple in design and operation, it lacks several qualities that make AFBG implementations more desirable. Overall bulk of this setup will likely increase manufacturing cost, as well as maintenance cost to ensure that there is no degradation in sensor performance due to loss of material from the buoy in the presence corrosive chemicals. Also, since this sensor is purely passive, adjustments to set-point and other measurement parameters are not possible unless the system is recalibrated. Finally, this implementation is very application specific and cannot be easily put to use in other applications. A high susceptibility to vibration exists due to the cantilever and float setup, preventing this implementation from being used where any type of motion of the vessel or liquid is involved.

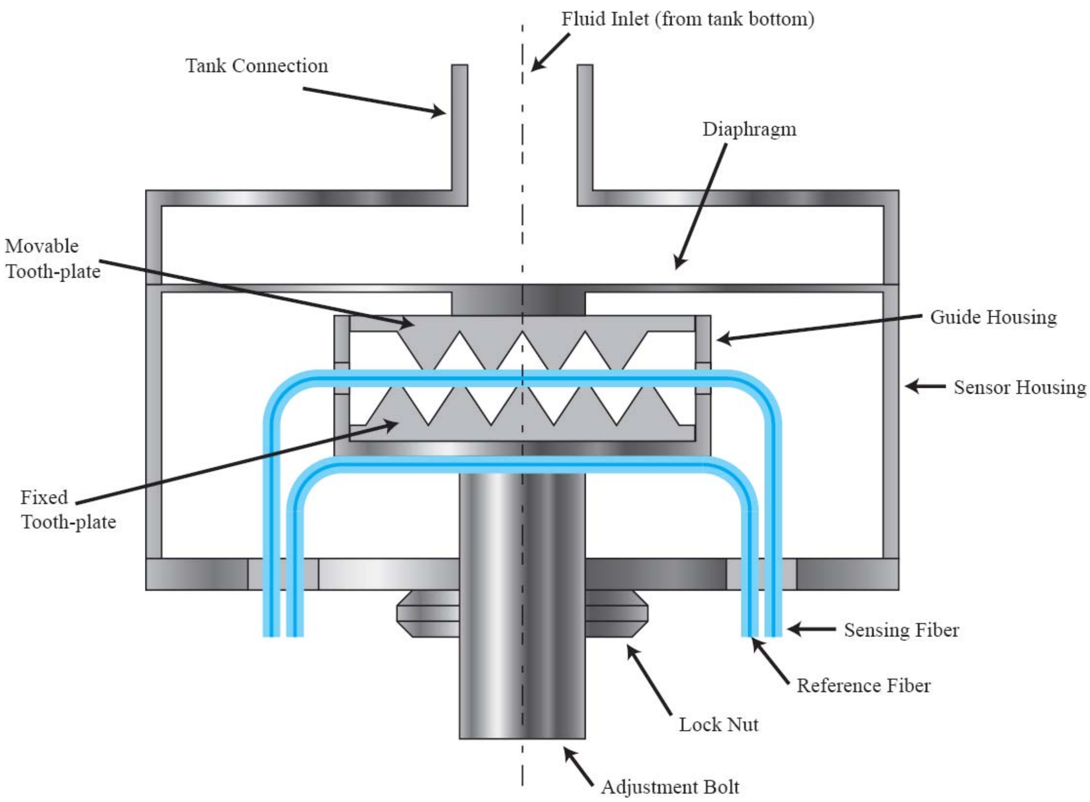

Figure 3.2.2 Illustration of the micro-bending liquid level sensor. [28]

The second sensor is also a mechanical type, applying stress to a section of optical fiber by means of a pair of tooth plates. Proposed by Gao *et al.* [28], this sensor relies on liquid pressure on a diaphragm to apply stress to a section of optical fiber. The diaphragm is placed in an opening on the bottom of the liquid vessel, allowing the weight of the liquid to provide level information. No grating is used for this setup but instead the period of the tooth plates combined with the micro-bending act together as a long-period grating. Liquid level information is obtained by monitoring light output from the fiber, which will be attenuated when higher order modes are coupled out of the fiber from the micro-bends induced in the fiber. A second fiber is also passed through the body of the sensor housing and monitored for light output as a reference to account for any fluctuations in the light source or fiber path to the sensor.

This is another application specific sensor implementation that would not easily be transferred to other sensing environments. As with the previous sensor, this sensor is relatively bulky and requires that existing liquid vessels be modified (and drained) so that the sensor may be fitted to the bottom. This sensor also has the disadvantage of poor performance in any environment where large temperature gradients and changes are present. Since most of the body of the sensor housing is metal, any change in temperature will cause a shift in sensor set point. In addition, this sensor requires a minimum of four feedthroughs for operation.

It is easy to see that fiber based mechanical sensors are desirable when considering a particular application, but limiting a sensor to only one application has the potential to increase costs for a customer if sensors performing similar functions are needed in different environments. To put it another way, it is desirable to have a sensor that functions the same in many environments with simple operation, a single signal / power feed through, immunity to EMI, and compact, affordable packaging. To take things a step further, several researchers have proposed several all fiber based sensors; however these also have their drawbacks when compared to AFBG technology. Some of these technologies include double-clad-like loss monitoring [29] where the liquid being measured acts as a second cladding and so affects the loss profile of the fiber, and reflection-based [30-32] sensing where the surface-air interface of the liquid is used as a reflecting medium to provide fluid level information. These sensors boast the same EMI immunity that is often desirable; however their operation may be somewhat complicated with each sensor often requiring a minimum of two fiber feedthroughs and occasionally the use of a lens [32] to couple light back into the receiving fiber. These factors add cost in both packaging and part count and also add a layer of complexity to the operation of the system. One approach mentioned here uses the concept of an evanescent field sensor [31] utilizing a Bragg grating inscribed with an ultra-fast laser. This approach is more along the lines of the AFBG concept; however the sensor must be fabricated on a section of pulled fiber with a diameter on the order of 30 – 50 μm. Considering that standard telecom fiber is around 125 μm (with jacket removed), this is a very small diameter. This sensor would be quite cost prohibitive since fabrication requires the use of an ultra-fast laser as well as expensive packaging due to the fragile nature of each grating.

The last sensor that will be examined utilizes a point array of diode sensors [33] to measure cryogenic liquids. This system is a good example of the technology currently used for cryogenic fuel monitoring in spacecraft. As the reader will see in Chapter 4, this is the primary designed application for the AFBG liquid level sensor. In the diode point array, a small pulsed current is passed through each diode and the voltage drop across each is measured. This voltage drop is proportional to the temperature of the surrounding medium. There is a high temperature contrast between the liquid and gas phases of any cryogenic fuel, which allows for a measurable difference in voltage drop across each sensor. For static level sensing (normal gravitational conditions, stationary vessel) a simple linear array of diodes will suffice. However, when this concept is implemented for a zero-G environment, the number of sensors required to adequately gauge the remaining fuel levels grows quite dramatically. In addition, many signal lines will be needed (minimum two per sensor) which also adds to the cost and complexity of the holding vessel. The higher required number of feedthroughs also introduces a higher potential for leakage and possible failure of the containment system. Also, it should be noted that this system is extremely vulnerable to EMI interference, which if picked up, becomes rectified and appears on the sensor output as an error. This is particularly true when long cable runs are involved, increasing the length of cable exposed.

All sensing systems previously mentioned in this section have two major drawbacks when compared to similar systems implemented with the use of an AFBG. Should any environmental conditions (temperature, pressure, etc) change, there is no way of actively adjusting the sensor to compensate for these effects. In many cases, a complete system recalibration is often needed. Also, complexity of the system is higher due to the need for multiple feedthroughs, should any of the sensors be placed on the inside of a liquid tank. By providing single feedthrough, EMI free operation, AFBG technology solves all of these difficulties in addition to being transferable to another sensing environment with no modifications.

3.3 THERMAL BASED VACUUM SENSOR

The second application of AFBGs presented in this manuscript is that of a thermal based vacuum sensor. Many advances in miniaturization of these sensors through the use of MEMS technology have been made based on existing methods of pressure sensing. Some of these methods include capacitive-based [34-36] gauges, Pirani-based thermal gauges [37-41], and thermocouple-based gauges [42]. Other approaches have also been presented including vacuum resonance gauges [43], and a fiber based thermal interferometer [44]. While most of these sensor types have their apparent advantages, their fabrication techniques and range of operation are somewhat prohibitive in application of this type of sensor, each design often being limited in range or size. In addition to fabrication and limited range, packaging requirements are likely to drive cost up, making these MEMS based sensors less appealing to industry.

Capacitive vacuum sensors rely on the change in capacitance between a stationary electrode and a moving diaphragm whose motion is affected by changes in pressure of a closed system. The sensitivity of capacitive vacuum sensors is not limited by the type of gas being measured, making them a desirable choice for any application. These sensors are not however, without their drawbacks. Commercialized capacitive vacuum sensors are often large and require a substantial amount of space for installation. Their large size presents a substantial thermal mass, requiring a minimum of 1 to 2 hours of stabilization time when heated to prevent the absorption of corrosive gasses [34]. In addition, costs in fabrication arise from difficulty in hermetic sealing of the capacitive cavity, particularly when attempting lead transfer from the sealed cavity to the outside environment [35]. Miniaturization of these devices through the use of MEMS technology has helped alleviate some of these problems; however there are still a few fundamental difficulties that cannot be avoided with this type of sensor design. In many cases, these sensors have a limited range and require varying designs or some sort of mechanical actuation to increase dynamic range [34]. Because the diaphragm is a movable part, the sensor is still susceptible to vibration despite its small size. In addition, fabrication is made more difficult by the need to prevent particle entry into the sensor, which would cause interference in vacuum measurement [34].

While the capacitive vacuum sensor may seem like an appealing sensor design, it is also easy to see the many drawbacks. AFBG based thermal vacuum sensors have the advantage of minimal packaging and fabrication costs. The sensor is small, and can be made quite responsive by the use of micro-structured fiber to enhance sensitivity, as the reader will see in Chapter 4. Additionally, only a single feed-through is required for operation and, if multiple sensing points are required, the creation of a multi-point sensing network is just a matter of adding more sensors to the fiber. The AFBG concept is a simple, robust design immune to EMI interference and suitable for harsh environments as well as situations where sustained high-rate acceleration and deceleration are common. Active tuning also allows for adjustment of set point and dynamic range, making this sensor ideal for a nearly unlimited range of pressures.

The capacitive-based vacuum sensor is a bit off the mark for comparison to AFBG-based sensors. Since the AFBG is a thermal-based device, it is more desirable to compare it to similar sensors that rely on thermal effects to gauge pressure. Typically, thermal based devices rely on interactions between a heat source and the gas molecules within the chamber being measured. The power required to keep the thermal element at a constant temperature is constantly monitored, this power being a function of thermal conductivity through the surrounding gas. As energy is carried away from the heat source through molecular collisions, the power required increases to maintain constant temperature. This increase is detected and registered as a change in pressure. Heat carried away from the thermal element is released via collisions with cooler surfaces within the chamber. As the molecular mean free path approaches a value less than that of the distance between the thermal element and chamber wall (or sensor casing), the heat conduction becomes non-linear and sensitivity begins to drop off [37, 38, 40]. Operation of this type of sensor is similar to a one-wire Pirani gauge.

Again it is relatively clear to see that this sensor has some inherent advantages, owing to its smaller size the benefit of MEMS technology. Silicon fabrication techniques have made miniaturization of these sensors a reality. There are however, several drawbacks. Due to the need for thermal isolation, suspended or free-standing parts are susceptible to mechanical shock and may easily break off within the device, making them unsuitable for high-G environments. Fabrication introduces higher cost due to violation of a number of design rules set forth in the standard IC process [38]. Because they rely on electrical connections for monitoring of pressure levels, they are also susceptible to EMI. All of these factors make the realization and implementation of AFBG-based thermal vacuum sensors more desirable.

Finally, a vacuum sensor design has been presented by Totsu *et al.* [44] which demonstrates nearly all of the sought-after qualities of the AFBG based design. In Totsu's design, a heated sensing element is fabricated on the end of a piece of standard telecom fiber. Using a Fabry-Perot effect, measurements of thermal conduction between the sensing element and surrounding gas (and hence pressure levels) are easily performed. This sensor boasts small size as well as immunity to EMI. This design however, is not without its drawbacks. Since the sensor is fabricated on the end of the fiber, it is not easily realized into a multipoint sensor network. Additionally, in order to avoid thermal drift of the sensor's output, the Fabry-Perot cavity must be attached to the fiber under vacuum. Along with the somewhat complicated fabrication process, this adds yet another layer of complexity to the design as well as increased cost. AFBG-based devices boast a simplistic design cycle, fulfilling all of the required features while keeping packaging and manufacturing costs low.

4.0 THERMAL BASED ACTIVE FIBER BRAGG GRATING SENSORS

This chapter presents two fundamental approaches to applications of fiber Bragg gratings for use as sensors. The first sensor involves the use of a multi-grating array for liquid level sensing at both room and cryogenic temperatures. These grating sensors were directly powered by in-fiber laser light. In-fiber diode laser light form a 910 nm diode laser array was coupled into the cladding of the fiber, where it was absorbed by an energy conversion coating at each of the sensing sites. With the laser off, the array functioned as a multi-point temperature sensor network. With the laser on, the power light heated the gratings, changing their fundamental resonance peak, allowing differentiation between liquid and gas phases. This grating array was experimentally evaluated for its ability to detect liquid levels at both room and cryogenic temperatures.

The second sensor is also based around an active fiber Bragg-grating and in-fiber light power delivery. The fundamental difference of this grating was that it was written in double clad fiber to help improve the efficiency of light delivery to the grating. For this setup, high power Argon-ion laser light (0.1 – 4 W) was coupled into the fiber. As in the previous setup, when the laser was turned off, the grating was used as a temperature sensor, allowing precise measurement of the temperature inside the vacuum chamber. With the laser on, the grating was used as a vacuum gauge by measuring the amount of spectral shift due to heat convection to the surrounding air. With more gas molecules, more convection was present, causing a smaller shift and hence a higher chamber pressure. Less gas molecules led to less convection, producing a sensor output corresponding to a lower chamber pressure. The sensor was able to accurately measure a pressure of 176 mTorr, at which point leaks in the chamber prevented any lower pressure testing. This sensor was evaluated in a constant power mode as well as a constant temperature mode at different pressures.

4.1 SELF HEATED FIBER BRAGG GRATING SENSORS

Liquid level sensing is often used in many applications to monitor the amount of liquid remaining in a vessel. Many industrial processes are critical to having a continuous supply of material (liquids in this case) on hand. Therefore this information is crucial to the continued operation of a process or, in the case of space travel, the outcome of a particular mission based on remaining fuel levels. The AFBG promises to realize a singe-fiber feedthrough sensing solution that surpasses all existing fiber and MEMS based technology by providing an EMI free device, while keeping costs low through the use of simple packaging.

This experiment sets out to realize an active fiber Bragg grating that can be directly powered by in fiber laser light. Fiber Bragg grating sensors powered by in fiber light operate on the principle that the power light is delivered through the same fiber as the sensing signal, as opposed to traditional tuning techniques. Along the length of the fiber, optical taps are created allowing high power laser light to be coupled into the cladding for use as an energy source for active tuning. This high-power light is then absorbed by an energy conversion coating on the outside of the active sensor, which allows for tuning by adjusting the power of the high-power light launched into the fiber. By eliminating delicate packaging, electrical cabling, and on fiber electrodes, Bragg grating enhancement can now be achieved without compromising any advantages of passive in-fiber sensors.

To demonstrate this concept, herein is presented a dual-function active fiber Bragg grating sensor array for liquid level and temperature sensing at both room and cryogenic temperatures. Current technology uses an array of silicon diode sensors for determining the temperature and liquid hydrogen levels inside cryogenic fuel tanks used in space missions. These diodes are heated using current pulses during operation. Since the voltage drop across each diode is temperature dependent, the temperature at any point in the array can be easily determined. When a diode is submerged in liquid hydrogen, the rise in temperature is limited by the boiling point of liquid hydrogen. A simple comparison of the temperature difference between submerged diodes and diodes outside the liquid can then utilized to determine liquid levels inside the tank. Due to the fact that liquid fuel does not settle to the bottom of a tank in a micro-gravity environment, a large number of sensors are needed to gauge the amount of fuel remaining in the fuel vessel. Each of these sensors requires two signal leads: one to supply current and another to measure the voltage drop. This requires a large number of feedthroughs for one tank, increasing heat leakage as well as the potential for both electrical and mechanical failure, especially in a high-G environment. In addition, these sensors are susceptible to electromagnetic interference, which becomes rectified and appears on the output as an error in the voltage drop measurement.

The problems presented above may be easily solved by the active-sensing technology proposed within this text. The dual function temperature and level sensor demonstrated here utilizes an active fiber Bragg grating array powered by in-fiber light. With no power light present, the multi-point sensor network of Bragg gratings may be used for precise measurement of the temperature distribution within the fuel tank. When power light is applied, optical energy carried by the fiber is used to heat each Bragg grating sensor in the network, allowing the network to distinguish between liquid and gas phases. The spectral thermal response of each sensor in the network is then detected and transmitted back through the same fiber which was used to deliver the power light. With the use of no wires and only one fiber feed through, this work promises a true single fiber solution for cryogenic level/temperature sensing.

4.1.1 Experimental Setup

The self-heated in-fiber sensor presented here was constructed from two sections of fiber as shown in figure 4.1.1 [45]. A single Bragg grating was first written into a standard piece of single-mode fiber, while the spectrum of this grating was monitored with an optical spectrum analyzer and a broadband source using a circulator. This fiber was then fusion-spliced to a second multimode fiber with a core diameter of 100-µm. A high-power laser diode array and a pair of 20x microscope objectives was then used to couple 10 watts of 910 nm laser light into the core of the multimode fiber. This high-power light propagating in the multi-mode fiber was then coupled into the cladding of the single-mode fiber at the splice junction due to mode mismatch between the two fibers. This coupling, or light leakage profile, was measured using the cut-back technique, which measures 910 nm light intensity as a function of distance from the splice. From these measurements, it was found that the light intensity leaking out from the fiber cladding falls off exponentially with distance from the junction. Within 10 cm of the splice junction, 90 percent of the light was lost. The Bragg grating was then plated with a uniform silver film to absorb the light leaking out of the cladding. The film had a resistance of 2.2 Ω/cm and began approximately 5 mm from the splice junction. All gratings used in the experiments had a uniform length of 10 mm.

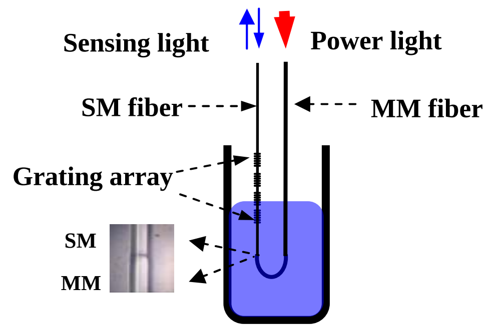

Figure 4.1.1 Sketch of grating level sensor array demonstrated in this work, Light from a high-power laser diode (LD) was focused by a 20× microscope objective (MO) and coupled into a multimode (MM) fiber, which is fusion spliced to the SM fiber. The actual fusion spliced SM to MM junction is shown in the inlet. [45]

After performing initial tests for liquid detection, this setup was further evolved to create a four point grating array to test liquid/gas discrimination by removing the array from the liquid one grating at a time. To realize this new array design, the 100/400 μm multi-mode fiber was replaced by a 62.5/125 μm (core/cladding) graded index (GRIN) fiber. This new fiber allowed the power light to propagate a greater distance from the splice junction, thereby allowing more sensors to be placed on a single fiber due to better mode matching.

4.1.2 Results

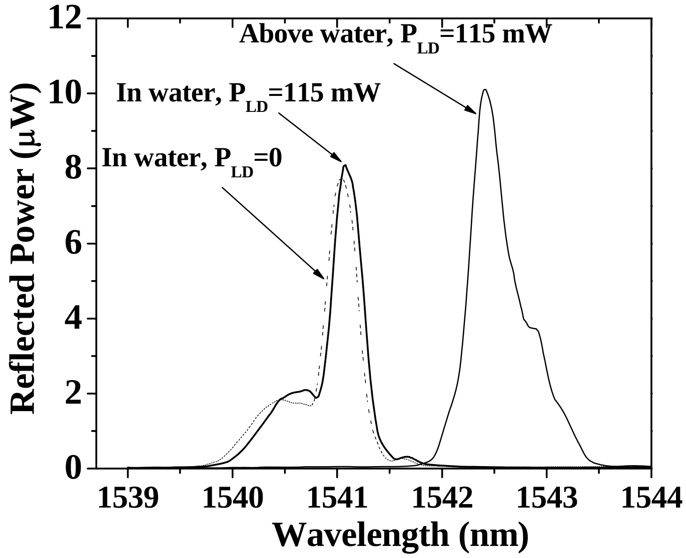

Figure 4.1.2 Bragg grating response in and out of water when heated by 115-mW 910-nm diode laser power.

Liquid sensing experiments for the first sensor were carried out in both water and liquid nitrogen. A spectral response for this grating in both water and air can be seen in figure 4.1.2, from which the basic operation of this sensor may be determined. With the laser off, the grating served as a temperature sensor, its changing spectral response showing the changing temperature of the surrounding medium. To determine whether or not the grating was submersed in liquid, the power laser was turned on, and 115 mW of power was injected to heat the grating. With the grating under water, the spectral response (solid trace) of this grating shifted about 60 pm from the un-heated trace (dotted trace). When the grating was removed from the water, this spectrum quickly shifted 1.4 nm from 1541 to 1542.1 nm. It should be noted that the reflection spectrum of the grating appears to have changed slightly, probably due to slight variations in thickness of the silver coating. Despite this slight discrepancy, the dramatic change of the resonance peak provided un-ambiguous detection of the location of the grating (liquid level). The differences in thermal responses of this grating are due to the stark differences in thermal properties of air and water. The thermal response of a similar grating in liquid nitrogen, water, and air as a function of input laser power may be seen in Figure 4.1.2. The grating exposed to air has, as expected, the greatest wavelength shift. This peak shift follows a linear trend versus input laser power with a slope of 15 pm / mW. Using this linear relationship, an input of 10 mW will produce a resonance peak (reflection peak) shift of 150 pm. This is a massive shift when compared to 20 pm for water and 5 pm for liquid nitrogen. The grating response for water and liquid nitrogen are also plotted on a reduced scale in an inset of the same figure. Since most liquids have a larger specific heat capacity and convection rate than that of air, it is more difficult to raise the temperature of a grating in liquid than in an air/gas environment. It should also be noted that when the temperature of the grating reaches the boiling point of the liquid in which it is immersed (77K for liquid nitrogen), the grating will be held at this temperature until all of the liquid has evaporated. This phenomenon may be seen in the inset of figure 4.1.2. The resonance peak of the grating initially shifted 20 pm and then remained constant over increasing injected power up to 680 mW while the same grating submerged in water increased to 170 pm with the same injected laser power.

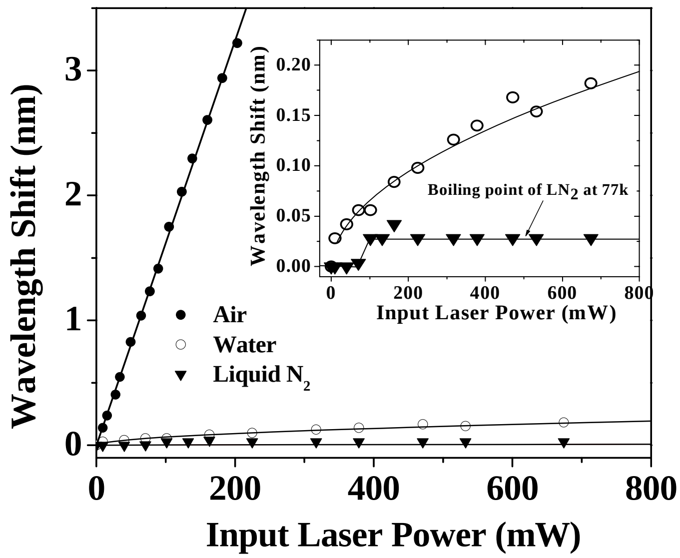

Figure 4.1.3 Resonance wavelength shifts of heated gratings in air, water, and liquid N2 as a function of input laser power. The grating wavelength shifts in water and liquid N2 re-plotted using a reduced vertical scale is shown in the inlet of the same figure.

For the demonstration of the four point Bragg grating sensor array, four 5 mm gratings were written in a single mode fiber (Corning SMF28). Each Bragg grating sensor was 3 cm apart with resonance wavelengths of 1535.6 nm (sensor 1), 1537 nm (sensor 2), 1538.8 nm (sensor 3), and 1540.6 nm. Sensor 4 was located approximately 4 cm from the splice junction. The reflection spectrum of the unheated grating array can be seen as the dot trace in figure 4.1.3. Sensor 4 (longest resonance wavelength) was the lowest sensor, while sensor 1 (shortest resonance wavelength) was the uppermost sensor. The reflection spectrum of the heated grating array may be seen in figure 4.1.3(a) which also shows the response when sensor 1 was above the water at 600 mW input power. The resonance peak of sensor 1 shifted from 1535.7 to 1536.05 (350 pm). The remaining sensors below the water shifted less than 10 pm due to the much larger specific heat capacity and thermal convection rates of water than that of air. For actual implementation of this sensor, much smaller wavelength shifts would be enough to ensure definite detection of liquid levels. Sensors 2, 3, and 4 showed similar behavior when removed from the water in series. Due to non-uniform leakage profile of the power light in single mode fiber, non-uniform peak shifts for each grating may be seen in figure 4.1.3(c) and 4.1.3(d) when the laser input power was reduced to 550 mW and 400 mW respectively. The power in these figures was reduced to prevent spectral deformation of sensor 4 due to overheating.

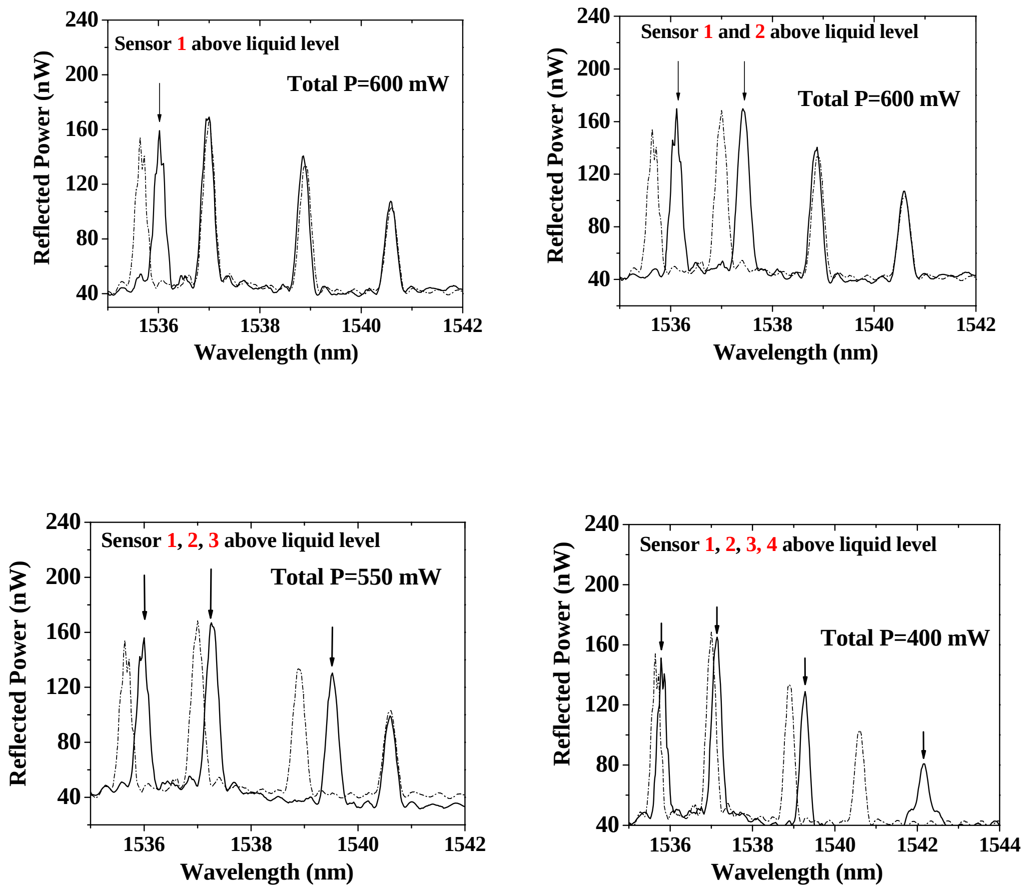

Figure 4.1.4 Spectral responses of a four-grating sensor array when the fiber was pulled out in series from water. Sensor 1 was the topmost grating and Sensor 4 was the lowest. The dot traces are the spectral responses for the unheated sensor.

4.1.3 Discussion

This work presents an ideal solution to not only power in-fiber components, but also to enhance their functionality in passive fiber sensor networks. These fibers are used for optical signal delivery as well as power light delivery for on fiber heating of in-fiber sensors. This idea of in-fiber light being used to power active fiber sensors provides groundwork to design responsive multifunction fiber sensors without sacrificing any of the inherent benefits of passive in-fiber sensors. In this work, an optically heated fiber Bragg grating was used to accurately determine liquid levels at both room and cryogenic temperatures. This sensor realization promises an ideal solution for cryogenic liquid fuel sensing in a microgravity environment. The optical energy delivered on the sensing fiber can also be used to power a number of other in-fiber sensors based on fiber Bragg gratings, micro-structure fiber, and fiber interferometers. It should be noted that in the configuration presented here, two fiber feedthroughs are still needed to deliver power light as well as an interrogation signal from each side of the grating sensor. This limitation may be overcome by the use of specialty double clad fibers. These fibers allow for sensing light at 1.55 μm to be launched along with the power light from only one end of the fiber. The double cladding also allows for longer propagation distances of the power light, thereby allowing longer and denser active fiber sensor networks. Demonstration of the use of double-clad fiber will be covered in the next section of this chapter.

4.2 FIBER BRAGG GRATING VACUUM SENSOR

Some of the most widely used instruments for vacuum measurement are thermal-based devices [46-48]. These devices, such as Pirani gauges, have seen a push over the past few years toward miniaturization using micro-electromechanical systems (MEMS) technology. Smaller sensors provide many advantages including improved dynamic response, higher measurement sensitivity, much lower power consumption, and low fabrication cost. However, these small sensors still require the same number of electrical feedthroughs, usually needing a flange with a nominal width of 1 to 2 inches. Some applications may arise where pressure information is needed at multiple points, such as in a spacecraft. In this case, many feedthroughs and vacuum flanges will be needed, further increasing the risk of leakage and mechanical failure. This leads to making the system more complex and also increases the cost significantly. In addition, many of the vacuum measurements are perturbation sensitive, and long cable runs from sensor to processing unit are often susceptible to electromagnetic interference leading to erroneous measurements.

This work presents an all-fiber thermal-based pressure gauge using fiber Bragg gratings. This solution requires no electrical cables, but instead uses only one fiber feed through and is based on the concept of active fiber components powered by in fiber laser light as presented in the pervious section. The thermal response of this optically heated grating was used to monitor the thermal response of the surrounding vacuum. This technology can be expanded to create a large vacuum sensor array using wavelength division multiplexing (WDM) or time division multiplexing (TDM) all while using a single fiber feed through. The work presented here promises a true one-fiber solution to vacuum and temperature sensing that is simple, light weight, responsive, and free from electromagnetic interference.

4.2.1 Experimental Setup

The vacuum sensor presented here was written in photo-sensitive double clad fiber, which has a germanium and phosphorus co-doped silica core. The germanium concentration in the core is 11 mole % with the core having a cutoff wavelength of 1450 nm. The fiber jacket is composed of a dual coating of UV curable acrylate with a final diameter of 245 μm. The innermost coating (closest to the fiber) has a refractive index lower than that of the pure silica fiber. This coating serves as the second cladding with a numerical aperture of 0.48, and a background loss of 2.3 dB / km at around 1100 nm. This inner cladding was used as the conduit to deliver high power laser light for on-fiber optical heating. In order to inscribe a Bragg grating into the core of this fiber, the cladding had to be carefully removed using methylene chloride. Using a standard phase mask technique, a 5 mm long apodized uniform Bragg grating was written in the fiber with a krypton-flourine (KrF) excimer laser operating at 248 nm. A silver coating, approximately 2 cm long and 0.2 μm thick was then plated over the Bragg grating located exactly in the center of the stripped fiber section. The double-clad fiber / grating assembly was then inserted into a vacuum calibration chamber and the ends passed through two vacuum feedthroughs. A rotary vane pump was used to control the pressure inside the chamber along with a mass flow controller to allow for pressure equalization once the chamber was pumped down. This also allowed for pressure control at higher vacuum levels where chamber pressure stabilization was difficult due to limitations in the chamber design. To monitor and calibrate the pressure inside the chamber, a convection gauge was installed next to the Bragg grating sensor. The grating response was monitored with an optical spectrum analyzer (Ando 6317C) and a broadband source in conjunction with a circulator connected to one end of the fiber.

Laser light from a high-power (0.1 – 4 W) multi-wavelength argon-ion laser was coupled into the inner cladding of the fiber using a 20x microscope objective with a coupling efficiency of over 90 %. With the argon laser off, the sensor was used to passively measure the temperature of the vacuum chamber. With the laser on, approximately 40% of the laser light propagating through the uncoated section of the fiber was absorbed by the silver coating. A uniform temperature gradient was then set up such that an un-distorted resonance wavelength shift of the Bragg grating was observed.

4.2.2 Results

The thermal response of a 5 mm Bragg grating at 173 mTorr may be seen in Figure 4.2.1. An input power of 145 mW caused a uniform shift of 2.0 nm at 173 mTorr. Despite the fact that the thermal coefficient of expansion of silver (5.5×10^{-6} K) is much larger than that of silica (0.66×10^{-6} K), the very thin film did not alter the thermal response of the Bragg grating significantly. With this in mind, the temperature rise of the heated section of the fiber was estimated at approximately 192 ºC (13 pm / $ºC^2$). Similarly, Pirani gauges and miniaturized MEMS vacuum sensors operate close to this temperature.

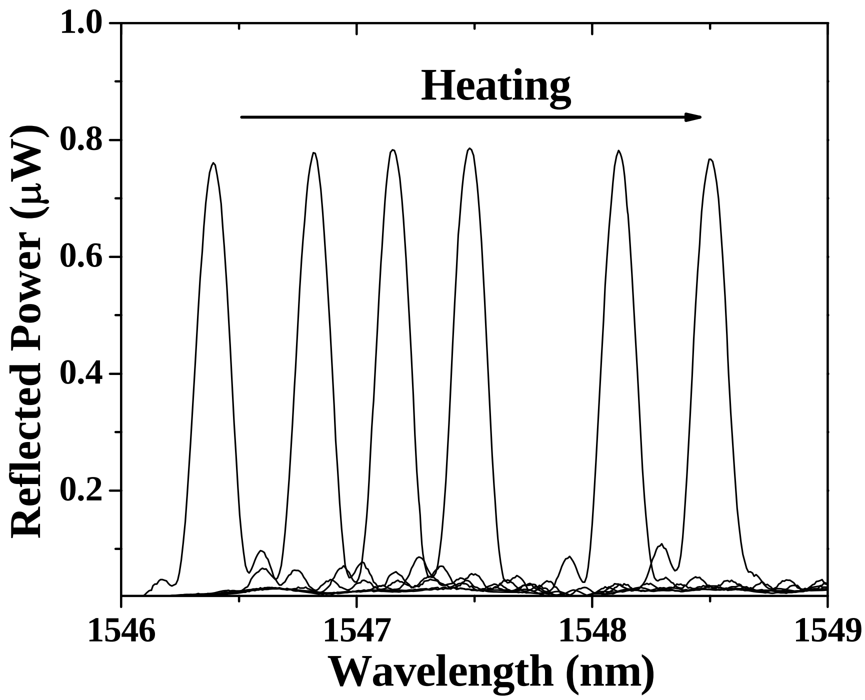

Figure 4.2.1 Resonance wavelength shift of a typical AFBG being optically heated at 173 mTorr. The powers used to heat the grating were 0, 10.5, 31, 52, 104, and 145 mW respectively.

The resonance wavelength shift of the Bragg grating versus coupled laser power may be seen in Figure 4.2.2. At higher temperatures, the thermal exchange between the silver and fiber enhance the thermal cooling rate of the fiber. Due to this higher heat conduction, higher laser powers (498 mW and 830 mW) are needed to shift the resonance wavelength the same amount (2.0 nm) at 6.3 and 749 Torr respectively.

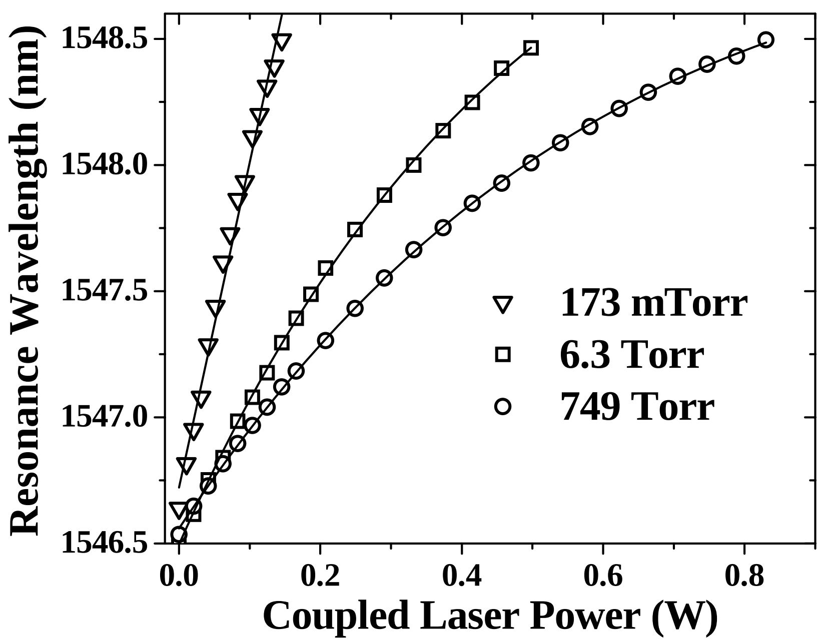

Figure 4.2.2 Resonance wavelength shift versus coupled power at 173 mTorr, 6.3 Torr, and 745 Torr respectively

Typically, most thermal-based vacuum sensors have two modes of operation: a constant resistance mode and a constant current mode. The Bragg grating sensor has two similar modes of operation: a constant temperature mode (similar to constant resistance) and constant power mode (similar to constant temperature). The Bragg grating sensor operating in constant power mode may be seen in Figure 4.2.3. The input power (from the argon-ion laser) was set to 145 mW and then 62 mW. With a chamber pressure of 173 mTorr, these input powers produced a shift in the peak resonant wavelength of the grating of 2.05 and 1.2 nm respectively. These input powers also produced a grating temperature rise of 179 ºC and 112 ºC.

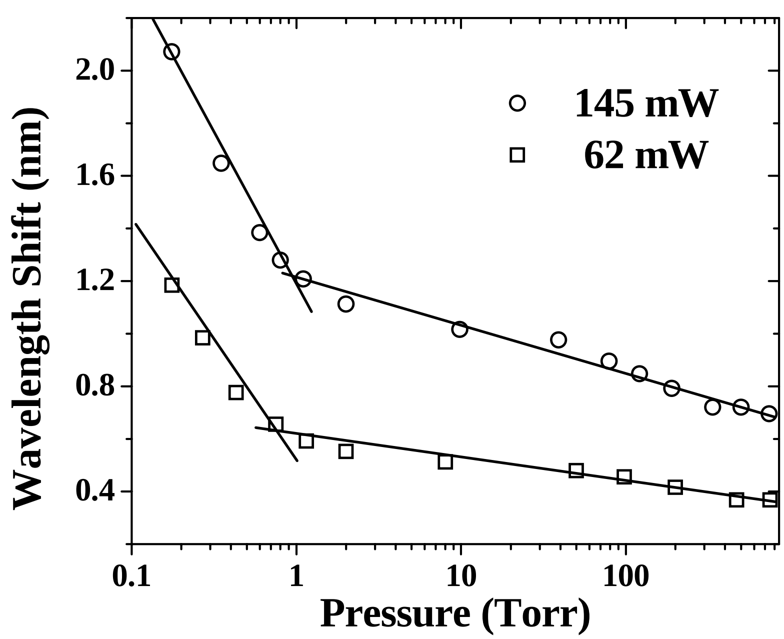

Figure 4.2.3 Vacuum sensor operating in constant power mode. The coupled laser powers are 62 mW and 145 mW respectively.

Figure 4.2.3 shows the resonant wavelength shift of the grating as a function of chamber pressure. Increasing chamber pressure caused a reduction in resonant wavelength shift due to the increase of thermal exchange due to convection between the heated fiber and the surrounding gas molecules. Figure 4.2.3 clearly shows that the sensor has two distinct regions of operation. For pressures below 1 Torr, the grating has a much higher sensitivity than for pressures above 1 Torr. When the pressure of the chamber was increased from 173 mTorr to 1 Torr, the grating wavelength shift corresponding to 145 mW of input power was reduced by 0.85 nm. This is in contrast with a reduction of only 0.44 nm for three orders of magnitude increase in chamber pressure (1 Torr to atmosphere). This response is similar to the behavior of typical thermal-based vacuum sensors operating in constant temperature mode. At low pressures (< 1 Torr), heat transfer is dictated by free molecular conduction, where the molecular mean free path is equal to or grater than the distance between the wall of the chamber and the heated grating. Heat is transferred from the grating to the gas and then from the gas to the wall of the chamber which is at a much lower temperature (room temperature). For pressure ranges less than 1 Torr, this process is proportional to the surrounding gas pressure in the chamber. For pressures above 1 Torr, heat transfer is dominated directly by convection between the heated fiber and the surrounding gas. This is a non-linear process, occurring at a much lower rate, and leads to reduced peak shifts in the resonance wavelength of the grating sensor. This problem of thermal convection can be solved by the use of on-fiber packaging or using micro-structured fibers to eliminate (or significantly reduce) this thermal exchange.

The sensitivity of this sensor can be actively tailored with in-fiber light, giving a fair demonstration of its dynamic range, which is also clearly shown in Figure 4.2.3. Choosing an input laser power of either 145 or 62 mW produces a resonance wavelength shift of 0.85 and 0.57 nm respectively, for pressures ranging from 173 mTorr to 1 Torr. A 49 % increase in responsivity of this sensor was produced by a 133 % increase in input laser power. However, in the 1 Torr to atmosphere range, the increase is more prominent. A shift of 0.22 nm at 62 mW input power to a 0.44 nm shift at 145 mW shows an increase in sensor responsivity of 100 %. Due to limitations of the vacuum system used for calibration, this sensor was unable to be tested at pressures below 174 mTorr. Traditional Pirani gauges having a thermal mass similar to that of the fiber used here can operate at pressures down to 10^{-3} Torr, and it is believed that this fiber sensor with a diameter of 125 μm will perform well at the same pressure.

As previously mentioned, this sensor has two modes of operation: constant power mode and constant temperature mode. Calibration in constant temperature mode was performed by increasing the input laser power to maintain the temperature (and resonance wavelength) of the optically heated grating. Results of this calibration can be seen in Figure 4.2.4, in which a grating with length 5 mm was heated by 150 and 350 mW input laser power. In this mode, the fiber sensor showed a single-exponential response to pressure. This is in contrast to the same grating operating in constant temperature mode, where two regimes of operation were seen. The cause for this difference in response between the two modes is not entirely clear. A nonlinear response was observed when the grating was heated with 350 mW input power over a pressure range of 3 to 200 Torr, most likely due to an increase in thermal convection to the surrounding gas at higher pressures, as with the previous mode of operation. In this mode, a 120 % increase in responsivity was seen from an increase in laser power from 249 to 538 mW (a 120 % increase).

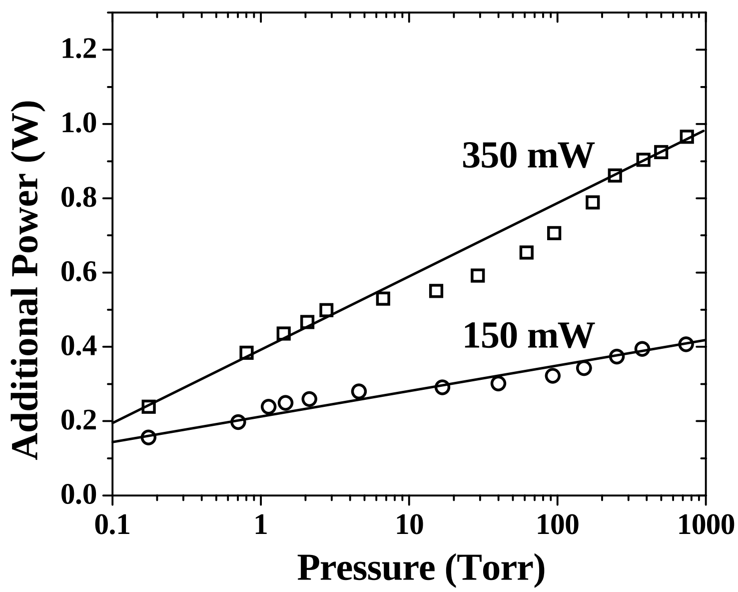

Figure 4.2.4 Operation of the FBG vacuum sensor in constant temperature mode. The grating was preheated with coupled laser powers of 150 and 350 mW respectively.

4.2.3 Discussion

The optically heated in-fiber vacuum sensor presented here utilized a double-clad specialty optical fiber with a diameter of 125 μm to enhance the capability to deliver power light to in-fiber sensors and allow power and signal light to be easily carried on the same fiber. Unfortunately, the response time of this sensor was slow owing to the fact that its excess thermal mass required large laser input powers for operation (50 – 500 mW). The large distance between the heated grating and the chamber wall allows for thermal convection to dominate at pressures greater than 1 Torr, which reduces the linearity and sensitivity. It is believed that these shortcomings may be overcome with the use of micro-structured optical fibers [15, 49]. In these specialty fibers, the air to core ratio is quite large owing to the fact that the core is surrounded by several large air holes that run the length of the fiber parallel to the core. The core is suspended from the walls of the inner fiber via thin ‘bridges’ of silica, with a cross section resembling that of an orange cut directly in half across the axis. A magnified picture of the cross section of this fiber can be seen in Figure 4.2.5. This fiber provides excellent thermal isolation between the core and the outer wall. In this case, only the core of the fiber would be heated, requiring much less optical power due to the reduced thermal mass of this ‘core-only’ configuration. Vacuum levels would then be measured by the thermal conduction between the heated fiber core and the shell of the fiber, the two of which are separated by less than 50 µm.

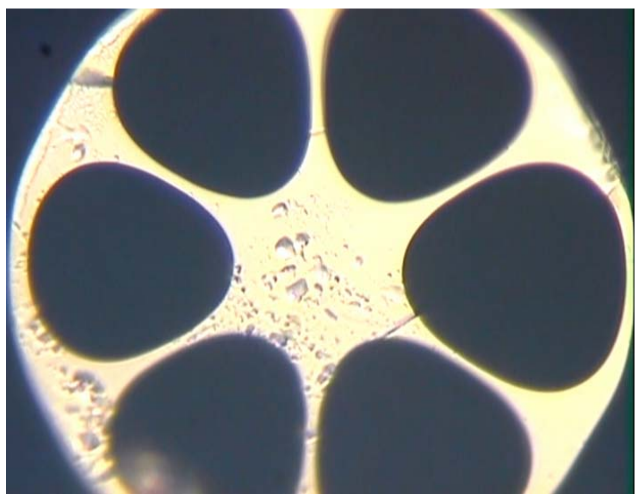

Figure 4.2.5 Magnified cross section of a micro-structured optical fiber.

Finally, this work demonstrates a solution to enhance the functionality of passive in-fiber sensors without sacrificing any of the benefits. In-fiber laser light was used to heat a fiber Bragg grating sensor which was used to measure both vacuum levels as well as temperature in a vacuum system. Temperature was measured passively when no power light was present, while applying power light allowed for active adjustment of sensor response to measure vacuum levels within the calibration system. This realization of an in-fiber based vacuum sensor was able to measure vacuum levels over four orders of magnitude. In addition, the double clad fiber used in this experiment allowed precise delivery of in-fiber power light to any point along the fiber. With the use of wavelength division multiplexing, the possibility for much improved multi-element vacuum / temperature sensor networks with the promise of a single feed through is quite prominent.

5.0 CONCLUSION AND SUMMARY

The work presented in this manuscript demonstrates significant advancements for the application of active fiber Bragg gratings in the role of sensing components. This new breed of sensing components allow for real-time adjustment of sensitivity, responsivity, dynamic range, and set point. The advancements in tuning via in-fiber laser light has allowed for long range sensor networks, which do not require bulky and expensive tuning mechanisms. Requiring a single feedthrough and being immune to electromagnetic interference are just a few of the many advantages that make this technology an ideal choice for almost any application. This is especially true if operating conditions require the need for a sensor with a long lifetime and the ability to operate in harsh conditions.

These concepts were presented in great detail in the form of two applications of AFBGs to fiber sensing technology. The first was that of a discrete liquid level sensing network, suitable for harsh conditions including dramatic changes in temperature and high and low G acceleration. This sensor network provided improvements over existing technology, allowing for a single fiber feedthrough, thus eliminating higher risk of leaks and/or vessel failure from higher numbers of feedthroughs. The second application was that of a fiber vacuum sensor. This sensor was demonstrated to have an equivalent response to similar Pirani-type vacuum gauges, but with the added advantage of faster response and smaller packaging size. In addition to showing an improvement in both size and cost over traditional MEMS based technology, this sensor was also able to perform multi-point networked sensing of vacuum levels. In addition to their dual-functions of temperature sensing along with liquid level / pressure sensing, these sensors were shown to be an excellent choice for sensing applications when compared to traditional fiber and MEMS based technology.

5.1 LIST OF RESULTING PUBLICATIONS

Journal papers:

[1] – Self-heated fiber Bragg grating sensors Chen, K.P. (Dept. of Electr. &; Comput. Eng., Univ. of Pittsburgh, PA, USA); McMillen, B.; Buric, M.; Jewart, C.; Wei Xu Source: Applied Physics Letters, v 86, n 14, 4 April 2005, p 143502-1-3

[2] – Fiber Bragg grating vacuum sensors McMillen, B. (Dept. of Electr. &; Comput. Eng., Univ. of Pittsburgh, PA, USA); Jewart, C.; Buric, M.; Chen, K.P.; Yuankun Lin; Wei Xu Source: Applied Physics Letters, v 87, n 23, 5 Dec. 2005, p 234101-1-3

5.2 FUTURE WORK

The work presented herein demonstrates several novel sensing functions based on active fiber Bragg grating technology. The applications, however, have been focused mainly on detection of changes in physical (environmental parameters). The future goal of this work is to extend the concept of AFBG-based sensing to the detection of chemicals in harsh environments. The first proposed application is that of leak detection and monitoring in hydrogen-based fuel delivery and storage systems.

Many air and space vehicles employ the use of hydrogen as a fuel, which requires that personnel who transport this fuel and the facilities in which it is stored are constantly exposed to potential hazards of fire and explosion. For this reason, leak detection is an important part in preventing these dangerous situations. Palladium has been demonstrated to provide excellent response to varying levels of hydrogen, specifically for chemical sensing [50]. Through the absorption of hydrogen, palladium hydrides are formed, which cause reversible physical (expansion) and chemical changes in the palladium. These changes have been shown to be detectable through a variety of electrical and optical means [51-58]. Palladium's sensitivity and response time, however, are severely degraded at extremely low temperatures (cryogenic systems) and low pressures (high altitudes). This is due to the fact that the formation of metal hydrides in palladium, and hydrogen diffusion / out-diffusion becomes very slow under these conditions [50]. AFBG-based sensing technology provides an excellent way to control localized temperature to within the desired optimal range, allowing for rapid diffusion and subsequent formation of palladium hydride in metal films for sensing. This control over temperature also allows for fast out-diffusion to reverse the process.

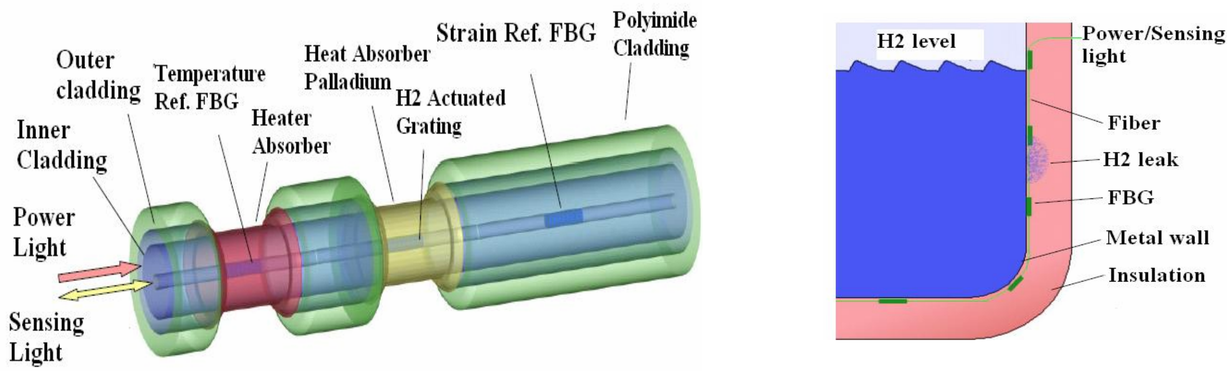

Figure 5.2.1 Illustration of a fiber-based hydrogen gas sensor composed of a palladium coated AFBG and two reference AFBGs (left) and an conceptual drawing of the installation of an active H_2 sensing network installed along a section of foam-insulated storage tank (right).

The combination of palladium hydrogen sensing along with AFBG technology allows for a one-fiber (and hence one feed through), arrayed, multifunction sensing system. This system also increases safety margins significantly since no electrical signals are involved with on-location sensing, meaning spark-free explosion proof operation. Control over the temperature of on-fiber palladium film promises dramatic improvement of the sensitivity and response time of fiber-based hydrogen sensors. An illustration of the proposed setup and installation may be seen in Figure 5.2.1. This work expands on the previously demonstrated fiber sensor arrays and use of double clad fiber for signal and power delivery. In this configuration, the outer cladding of the fiber is removed exposing the inner cladding. Metal films (such as palladium) are then sputter coated onto this exposed section of fiber. The presence of the metal film causes a disturbance in the waveguide profile, causing a small amount of power light (which is carried in the inner cladding double clad fiber) is tapped out and absorbed by the palladium film. The heat absorbed causes a small spectral shift of the resonance wavelength of the grating, which will be further shifted upon absorption of hydrogen by the palladium film. In order to detect differences between hydrogen absorption and temperature and/or applied strain, two secondary FBGs will be added before and after the hydrogen sensor section of the fiber. One of these FBGs will contain an ordinary energy conversion coating (not sensitive to hydrogen) providing a temperature reference, while the other will be left uncoated, providing a strain reference.

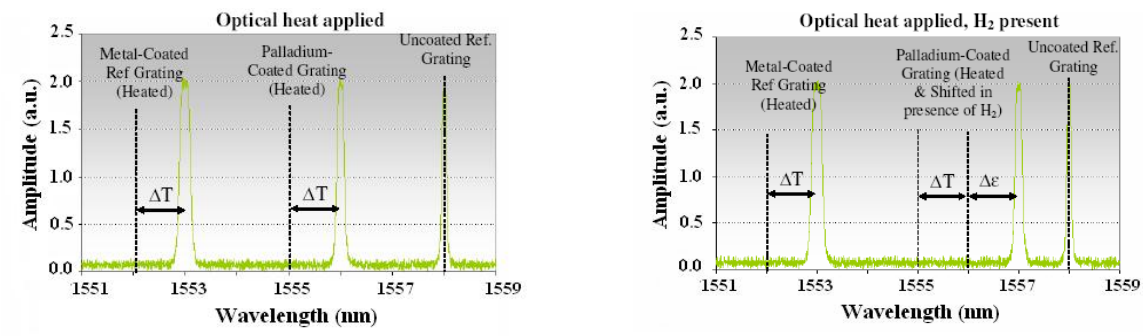

Figure 5.2.2 Initial experimental results for a palladium-based hydrogen sensor. The left-hand plot shows initial heating of the 3-sensor array (palladium sensor and two reference gratings) shifted by optical heating (60°C). No hydrogen was present in this plot. The right-hand plot shows the same plot as the right, only with a 4% (volume %) of hydrogen in the chamber atmosphere.

Figure 5.2.2 shows preliminary results of initial tests of AFBG based hydrogen sensor response to the presence of hydrogen, which was done in collaboration with Lakeshore Cryotronics Inc. The center FBG is coated with approximately 1 μm of palladium film, the left-hand FBG is coated with aluminum (temperature reference), and the right-hand FBG is left uncoated (strain reference). The additional center FBG shift, seen in the right-hand plot, is due to the palladium film absorbing hydrogen present in the ambient gas mixture. This absorption causes the palladium film to swell, inducing strain on the sensing grating, producing the additional shift seen in Figure 5.2.2.

Based on this preliminary work, future research efforts will involve improvements to the design and operation of palladium based AFBG sensors. Baseline responses and sensitivities must be established for varying palladium film thicknesses at different temperatures in order to find an optimal response. This optimal response will be based around the best projected hydrogen sensitivity of 1% (volume %). From here, efforts will be directed toward determining the temperature dependence of these sensitivities. This will allow studies of the feasibility of temperature induced de-sorption of hydrogen. Once a baseline for optimal hydrogen sensing has been established, AFBG chemical sensing will be extended to include moisture detection based on hydrophilic polymer coatings. Similar to the palladium coatings, these polymers expand when water is absorbed, and if applied to an FBG, will produce an induced shift based on the amount of moisture absorbed. Using this same principle, sensing methods for other chemicals (both gas and the vapors of volatile chemicals such as kerosene and gasoline) will also be developed.

BIBLIOGRAPHY

[1]. K. O. Hill, Y. Fujii, D. C. Johnson, and B. S. Kawasaki, *Photosensitivity in optical fiber waveguides: Application to reflection filter fabrication*. Appl. Phys. Lett., 1978. **32**(10): p. 647-649.

[2]. B. S. Kawasaki, K. O. Hill, D. C. Johnson, and Y. Fujii, N*arrow-band Bragg reflectors in optical fibers*. Opt. Lett., 1978. **3**: p. 66.

[3]. Feng, K.-M., et al., *Tunable nonlinearly-chirped fiber Bragg grating for use as a dispersion compensator with a voltage-controlled dispersion in Optical Fiber*. Communication Conference and Exhibit, 1998. OFC '98.

[4]. Rogers, J.A., et al., *Distributed on-fiber thin film heaters for Bragg gratings with adjustable chirp.* Appl. Phys. Lett., 1999. **74**(21): p. 3131 - 3133.

[5]. Limberger, H.G., et al., *Efficient miniature fiber-optic tunable filter based on intracore Bragg grating and electrically resistive coating.* Photonics Technology Letters, IEEE, 1998. **10**(3): p. 361-363.

[6]. Doyle, A., et al., *FBG-based multi-channel low dispersion WDM filters.* Electronics Letters, 2002. **38**(24): p. 1561-1563.

[7]. Yeom, D.I., H.S. Park, and B.Y. Kim, *Tunable narrow-bandwidth optical filter based on acoustically modulated fiber Bragg grating.* Photonics Technology Letters, IEEE, 2004. **16**(5): p. 1313-1315.

[8]. Nykolak, G., et al., *All-fiber active add-drop wavelength router.* Photonics Technology Letters, IEEE, 1997. **9**(5): p. 605-606.

[9]. Chen, K.P., L.J. Cashdollar, and W. Xu, *Controlling Fiber Bragg Grating Spectra with in-fiber Diode Laser Light.* Photonics Technology Letters, IEEE, 2004. **16**(8): p. 1897 – 1899.

[10]. Goh, Chee S.; Set, Sze Y.; Kikuchi, Kazuro; Ibsen, Morten; Mokhtar, M.R.; Butler, S.A., *Wavelength tuning of fiber Bragg gratings over 90 nm using a simple tuning package*. Photonics Technology Letters, IEEE, 2003. **15**(4): p. 557-559 .

[11]. G. R. Fox, C. A. P. Muller, N. Setter, D. M. Costantini, N. H. Ky, and H. G. Limberger, *Wavelength tunable fiber Bragg grating devices based on sputter deposited resistive and piezoelectric coatings.* J. Vac. Sci. Technol. A, 1997. **15**: p. 1791-1795.

[12]. P. Mach, T. Krupenkin, S. Yang, and J. A. Rogers, *Dynamic tuning of optical waveguides with electrowetting pumps and recirculating fluid channels.* Appl. Phys. Lett., 2002. **81**(2): p. 202–204.

[13]. John A. Rogers, Benjamin J. Eggleton, Janet R. Pedrazzani, and Thomas A. Strasser, *Distributed on-fiber thin film heaters for Bragg gratings with adjustable chirp.* Appl. Phys. Lett., 1999. **74**(21): p. 3131-3133.

[14]. Limberger, H.G.; Nguyen Hong Ky; Costantini, D.M.; Salathe, R.P.; Muller, C.A.P.; Fox, G.R., *Efficient miniature fiber-optic tunable filter based on intracore Bragg grating and electrically resistive coating*. Photonics Technology Letters, IEEE, 1998. **10**(3): p. 361-363.

[15]. P. Mach, M. Dolinski, K. W. Baldwin, J. A. Rogers, C. Kerbage, R. S. Windeler, and B. J. Eggleton, *Tunable microfluidic optical fiber.* Appl. Phys. Lett., 2002. **80**(23): p. 4294 – 4296.

[16]. Andreas Othonos, *Fiber Bragg gratings.* Rev. Sci. Instrum., 1997. **68**(12): p. 4309 – 4341.

[17]. Kassap, S. O. (2001), *Optoelectronics and Photonics*, 2001, Upper Saddle River NJ: Prentice-Hall Publishing

[18]. Othonos, A. and K. Kalli, *Fiber Bragg Gratings, Fundamentals and Applications in Telecommunications and Sensing*, 1999, Norwood USA: Artech House Publishing

[19]. M. J. Yuen, *Ultraviolet absorption studies of germanium silicate glasses.* Appl. Opt., 1982. **21**(1): p. 136-140.

[20]. D. K. W. Lam and B. K. Garside, *Characterization of single-mode optical fiber filters.* Appl. Opt., 1981. **20**(3): p. 440-445.

[21]. J. Stone, *Photorefractivity in* GeO_2*-doped silica fibers.* J. Appl. Phys., 1987. **62**(11): p. 4371-4374.

[22]. G. Meltz, W. W. Morey, and W. H. Glenn, *Formation of Bragg gratings in optical fibers by a transverse holographic method.* Opt. Lett., 1989. **14**(15): p. 823-825.

[23]. D. P. Hand and P. St. J. Russell, IOOC, Technical Digest, Japan, 1989. :p. 21C3 – 21C4.

[24]. Chakravarthy, S.; Sharma, R.; Kasturi, R., *Noncontact level sensing technique using computer vision Source.* IEEE Transactions on Instrumentation and Measurement, 2002. **15**(2): p. 353-361.

[25]. Donlagic, D., *A robust miniature acoustical liquid level gauge with micrometer resolution.* Review of Scientific Instruments, 2002. **73**(2): p. 464-467.

[26]. Seoktae Kim; Cam Nguyen, *A displacement measurement technique using millimeter-wave interferometry.* IEEE Transactions on Microwave Theory and Techniques, 2003. **51**(6): p. 1724-1728.

[27]. Tuan Guo; Qida Zhao; Qingying Dou; Hao Zhang; Lifang Xue; Guiling Huang; Xiaoyi Dong, *Temperature-insensitive fiber Bragg grating liquid-level sensor based on bending cantilever beam*. Photonics Technology Letters, IEEE, 2005. **17**(11): p. 2400-2402.

[28]. Gao, J.Z.; Zhao, Y.L.; Jiang, Z.D., *Design and performance characterization of a fibre optical sensor for liquid level monitoring.* Journal of Physics: Conference Series, 2005. **12**(1): p. 77-80.

[29]. Perez-Ocon, F.; Rubino, M.; Abril, J.M.; Casanova, P.; Martinez, J.A., *Fiber-optic liquid-level continuous gauge.* Sensors and Actuators A (Physical), 2006. **125**(2): p. 124-132.

[30]. Musayev, E.; Karlik, S.E., *A novel liquid level detection method and its implementation.* Sensors and Actuators A (Physical), 2003. **A109**(1-2): p. 21-24.

[31]. Grobnic, D.; Mihailov, S.J.; Huimin Ding; Smelser, C.W., *Bragg grating evanescent field sensor made in biconical tapered fiber with femtosecond IR radiation.* Photonics Technology Letters, IEEE, 2006. **18**(1): p. 160-162.

[32]. Vazquez, C. (Escuela Politecnica Superior, Univ. Carlos III Madrid, Spain); Garcinuno, J.; Pena, J.M.S.; Gonzalo, A.B., *Multi-sensor system for level measurements with optical fibres.* IECON - 28th Annual Conference of the IEEE Industrial Electronics Society, 2002. **4**: p. 2657-2662.

[33]. Van Dresar, N.T., *PVT gauging with liquid nitrogen.* Cryogenics, 2006. **46**(2-3): p. 118-125.

[34]. Miyashita, H.; Esashi, M., *Wide dynamic range silicon diaphragm vacuum sensor by electrostatic servo system Source.* Journal of Vacuum Science & Technology B (Microelectronics and Nanometer Structures), 2000. **18**(6): p. 2692-2697.

[35]. Yafan Zhang; Massoud-Ansari, S.; Guangqing Meng; Woojin Kim; Najafi, N. *An ultra-sensitive, high-vacuum absolute capacitive pressure sensor.* MEMS 2001 14th IEEE International Conference on Micro Electro Mechanical Systems, 2001. p. 166-169.

[36]. Chavan, A.V.; Wise, K.D, *A batch-processed vacuum-sealed capacitive pressure sensor*. Tranducers 97. 1997 International Conference on Solid-State Sensors and Actuators. Digest of Technical Papers, 1997, pt. 2, **vol. 2**: p. 1449-1452.

[37]. Klaassen, E.H.; Kovacs, G.T.A., *Integrated thermal conductivity vacuum sensor.* Solid-State Sensor and Actuator Workshop, 1996: p. 249-252.

[38]. Paul, O.; Baltes, H., *Novel fully CMOS-compatible vacuum sensor.* Sensors and Actuators A (Physical), 1995. **A46**(1-3): p. 143-146.

[39]. Berlicki, T.M., *Thermal vacuum sensor with compensation of heat transfer.* Sensors and Actuators A (Physical), 2001. **A93**(1): p. 27-32.

[40]. Alvesteffer, W.J.; Jacobs, D.C.; Baker, D.H., *Miniaturized thin film thermal vacuum sensor.* Journal of Vacuum Science & Technology A (Vacuum, Surfaces, and Films), 1995. **13**(6): p. 2980-2985.

[41]. Chou, B.C.S.; Yeong-Maw Chen; Mang Ou-Yang; Jin-Shown Shie, *A sensitive Pirani vacuum sensor and the electrothermal SPICE modeling.* Sensors and Actuators A (Physical), 1996. **A53**(1-3): p. 273-277.

[42]. Chatterjee, S.; Halder, A.K.; Sengupta, K.; Maiti, H.S., *A vacuum gauge using positive temperature coefficient thermistor as the sensor.* Review of Scientific Instruments, 2000. **71**(12): p. 4670-4673.

[43]. Gutierrez, R.C.; Tang, T.K.; Stell, C.B.; Vorperian, V.; Shcheglov, K., *Bulk micromachined vacuum sensor.* Tranducers 97. International Conference on Solid-State Sensors and Actuators. Digest of Technical Papers, 1997. pt. 2, **vol.2**: p. 1497-1500

[44]. Totsu, K.; Haga, Y.; Esashi, M., *Vacuum sealed ultra miniature fiber-optic pressure sensor using white light interferometry.* TRANSDUCERS '03. 12th International Conference on Solid-State Sensors, Actuators and Microsystems. Digest of Technical Papers, 2003, pt. 1, **vol.1**: p. 931-934.

[45]. Chen, Kevin P.; Cashdollar, Lucas J.; Xu, Wei, *Controlling fiber Bragg grating spectra with in-fiber diode laser light.* Photonics Technology Letters, IEEE, 2004. **16**(8): p. 1897-1899.

[46]. Wilferf, St.; Edelmann, Chr., *Miniaturized vacuum gauges*. Journal of Vacuum Science and Technology A: Vacuum, Surfaces and Films, 2004. **22**(2): p. 309-320.

[47]. Wang, S.N.; Mizuno, K.; Fujiyoshi, M.; Funabashi, H.; Sakata, J., *Thermal micropressure sensor for pressure monitoring in a minute package.* Journal of Vacuum Science & Technology A: Vacuum, Surfaces, and Films, 2001. **19**(1): p. 353-357 .

[48]. Alvesteffer, W.J.; Jacobs, D.C.; Baker, D.H., *Miniaturized thin film thermal vacuum sensor.* Journal of Vacuum Science & Technology A: Vacuum, Surfaces, and Films, 1995. **13**(6): p. 2980-2985.

[49]. Kerbage, C.; Steinvurzel, P.; Reyes, P.; Westbrook, P.S.; Windeler, R.S.; Hale, A.; Eggleton, B.J., *Highly tunable birefringent microstructured optical fiber.* Optics Letters, 2002. **27**(10): p. 842-844.

[50]. Lewis, F.A., *The Palladium Hydrogen System.* Academic Press, London, 1967.`

[51]. D'Amico, A.; A. Palma; and E. V*erona, Palladium surface acoustic wave interaction for hydrogen detection.* Appl. Phys. Lett., 1982. **41**(3): p. 300-301.

[52]. Steele, M.C.; B.A. MackIver, *Palladium/cadmium-sulfide Schottky diodes for hydrogen detection.* Appl. Phys. Lett., 1976. **28**(11): p. 687-688.

[53]. Lundstrom, I.; S. Shivaraman; C. Svensson; L. Lundkvist, *A hydrogen–sensitive MOS field–effect transistor.* Appl. Phys. Lett., 1975. **26**(2): p. 55-57.

[54]. Favier, F.; E.C. Walter; M. P. Zach; T. Benter; R.M. Penner, *Hydrogen Sensors and Switches from Electrodeposited Palladium Mesowire Arrays.* Science, 2001. **293**(5538), p. 2227-2231.

[55]. X. Bevenot; A. Trouillet; C. Veillas; H. Gagnaire; and M. Clement, *Hydrogen leak detection using an optical fibre sensor for aerospace applications.* Sen. & Act. B, 2000. **56**(1-2): pp. 158-163.

[56]. X. Bevenot; A. Trouillet; C. Veillas; H. Gagnaire; and M. Clement, *Surface plasmon resonance hydrogen sensor using an optical fiber.* Meas. Sci. Technol., 2002. **13**(1): p.118-124.

[57]. Tabib-Azar, M.; B. Sutapu; R. Petrick; A. Kazemi, *Highly sensitive hydrogen sensors using palladium coated fiber optics with exposed cores and evanescent field interactions.* Sens. Act. B, 1999. **56**(1-2): p. 158-163.

[58]. Villatoro, J. D. Monzon-Hernandez, "Fast detection of hydrogen with nano fiber tapers coated with ultra thin palladium layers" Optics Expr., 2005. **13**(13): p. 5087-5092.